2014-01-1255
Published 04/01/2014

doi:10.4271/2014-01-1255
saeeng.saejournals.org

In-Cylinder Mechanisms of Soot Reduction by Close-Coupled Post-Injections as Revealed by Imaging of Soot Luminosity and Planar Laser-Induced Soot Incandescence in a Heavy-Duty Diesel Engine

Jacqueline O'Connor
Pennsylvania State Univ.

Mark Musculus
Sandia National Labs.

ABSTRACT

Post injections have been shown to reduce engine-out soot emissions in a variety of engine architectures and at a range of operating points. In this study, measurements of the engine-out soot from a heavy-duty optical diesel engine have conclusively shown that interaction between the post-injection jet and soot from the main injection must be, at least in part, responsible for the reduction in engine-out soot. Extensive measurements of the spatial and temporal evolution of soot using high-speed imaging of soot natural luminosity (soot-NL) and planar-laser induced incandescence of soot (soot-PLII) at four vertical elevations in the piston bowl at a range of crank angle timings provide definitive optical evidence of these interactions.

The soot-PLII images provide some of the most conclusive evidence to date that the addition of a post injection dramatically changes the topology and quantity of in-cylinder soot. As the post jet penetrates toward the bowl wall, it carves out regions from the main-injection soot structures, either through displacement of the soot or through rapid and progressive oxidation of the soot. Later in the cycle, the regions of main-injection soot on either side of the jet centerline, clearly present in the main-injection-only case, have all but disappeared when the post-injection is added - only the soot in the post-injection pathway remains. Evidence of this apparent late-cycle oxidation of main-injection soot appears in both the soot-PLII and soot-NL images, providing substantial support for the mixing mechanism of soot reduction with post injections. Implications of these findings and future work are also discussed.

CITATION: O'Connor, J. and Musculus, M., "In-Cylinder Mechanisms of Soot Reduction by Close-Coupled Post-Injections as Revealed by Imaging of Soot Luminosity and Planar Laser-Induced Soot Incandescence in a Heavy-Duty Diesel Engine," *SAE Int. J. Engines* 7(2):2014, doi:10.4271/2014-01-1255.

INTRODUCTION

Modern heavy-duty diesel engines can meet pollutant emissions targets using a variety of strategies [1, 2]. Approaches include multi-stage aftertreatment systems [3], modification to the combustion mode to achieve various degrees of low-temperature combustion (LTC) [4], and advanced fuel-injection schemes [5, 6], including multiple-injection schedules and injection rate-shaping. In this study, we address the use of multiple injections, post-injections in particular, to control particulate emissions from heavy-duty diesel engines.

Post injections can be an effective way to reduce engine-out soot emissions for a variety of engine sizes and at a wide range of operating conditions. Measurements of post-injection efficacy have been published in numerous studies; for a more detailed review, see O'Connor and Musculus [7]. These studies have shown that post-injection efficacy is sensitive to several key operating parameters, including injection timing, load, exhaust gas recirculation (EGR), speed, and fuel-spray targeting.

Proposed mechanisms for engine-out soot reduction with post injections generally fall into three categories. First, several studies [5, 6, 8, 9, 10, 11, 12, 13, 14, 15, 16, 17, 18, 19, 20] have identified an enhanced mixing mechanism as the driver of engine-out soot reduction. Some authors have attributed the engine-out soot reductions to enhanced mixing of the main-injection soot with air entrained by the post injection, which increases oxidation rates of main-injection soot [8, 9, 12, 17, 19]. Alternatively, other authors [14] have indicated that the post injection enhances mixing of ambient air with fuel and/or

combustion intermediates, from both the main and post injection, thereby reducing the local equivalence ratio and suppressing local soot formation.

Second, several authors have proposed a thermal mechanism by which the combustion of the post injection increases local temperatures, thereby enhancing oxidation of main-injection soot and reducing overall soot emissions [5, 8, 21, 22, 23, 24, 25, 26]. Temperature effects on soot oxidation are difficult to verify experimentally, but two-color pyrometry measurements [27] and predictive simulations [12] have indicated increased soot temperatures with post injections, which is consistent with the proposed thermal mechanism.

Finally, a small number of studies have indicated that engine-out soot may be a function of injection duration and not simply total mass of fuel injected [19, 28, 29, 30, 31]. According to these studies, soot formation during an injection is a non-linear function of the duration of the injection. Consequently, a given quantity of fuel will form less soot if it is delivered in several short injections instead of a single large injection. Sometimes referred to as the “split-flame” concept [29, 30], this hypothesis has mostly been proposed for multiple-injection schedules with a very short dwell between injections. Other studies refer to the fundamental mechanism behind duration-dependent soot formation as “jet replenishment” [28].

Despite the prevalence of these three explanations in the literature, there are few studies that provide direct experimental or computational evidence of these mechanisms or quantify the relative importance of each fundamental mechanism by which post injections reduce engine-out soot. This lack of data is driven by the complexity of the problem; not only are in-cylinder mixing fields and temperatures difficult to measure, the mechanism by which soot is reduced by post injections may vary with operating condition [32], creating a virtually endless experimental design space.

In particular, the extent of the interaction between the post jet and the main-injection mixture is difficult to quantitatively measure in engine environments. Several spray-vessel experiments have used scalar mixing and front-tracking techniques to quantitatively measure the interaction between multiple injections [33, 34, 35]. While these studies provide valuable information about the freely-propagating regime of the spray, the boundary conditions of these experiments do not faithfully represent those in an engine environment. In particular, the lack of jet impingement and subsequent roll-up at the bowl wall makes it difficult to extrapolate these results to an engine geometry. Indeed, in current production engines that use post-injections, soot-reduction efficacy is known to be strongly dependent on spray targeting and/or piston geometry [7, 36]. Further, two of the three theories of soot reduction using post injections - the enhanced mixing and thermal mechanisms - are dependent on the interaction between the post jet and the main-injection products. Hence, interactions of both the main jet and post jet with the engine geometry are key to understanding the mixing field. For the mixing mechanism, the post injection transports oxygen to oxidizer-starved regions, either suppressing soot formation as the main-injection fuel is burning, or enhancing soot oxidation after soot has formed from the main-injection fuel. For the thermal mechanism, interaction of the reacting post jet with the main-injection products raises local temperatures, enhancing oxidation of soot from the main- and/or post-injection combustion. In either case, the details of the interaction between the post jet and the main-injection mixture clearly are important, but are difficult to measure.

In our previous work [32, 37], we have made an initial attempt to understand the interaction between the post jet and the main-injection soot in a heavy-duty optical diesel engine using high-speed soot natural luminosity imaging (soot-NL) and phase-resolved (one image per cycle at a selected crank angle) soot planar laser-induced incandescence (soot-PLII) along the spray axis. From these data, it was clear that the post jet interacted with the main-injection mixture, where interactions appeared to include displacement of the main-injection mixture by the post jet, entrainment of some of the residual main-injection jet by the post jet, and merging of the post-injection mixture with the main-injection mixture in the rotating soot structures on either side of the jet centerline. The magnitude of these effects varied with main-injection duration and post-injection duration. These effects may have also changed with intake-oxygen level; however, as discussed in Ref. [32], we were unable to track fluid motion and mixing using soot-NL imaging at very low intake-oxygen levels (12.6%-15%).

While the observations in these studies confirmed that interaction between the post jet and the main-injection products was associated with engine-out soot reduction, both the spatial and temporal details of the interaction were difficult to discern as a result of the limited data available. While the soot-NL videos provided a fast frame rate that allowed visualization of the evolving soot structures, this line-of-sight integrated data did not resolve the vertical location of the soot and fluid structures that drive the interaction between the post jet and main-injection products. Although complementary soot-PLII data helped to unravel some of the line-of-sight issues, data were only available within one plane, and soot distributions within the full three-dimensional field not intersected by the laser sheet could be quite important during these interactions. The goal of the current study is to acquire soot-PLII data at multiple elevations from the firedeck to map the evolution of soot in both space and time over a greater extent of the combustion chamber.

In this study, we have limited the operational space to low-load, conventional diesel operation with 18% intake-oxygen (20-30% EGR) at a single speed and boost. In our previous studies [32, 37], we mapped the injection-timing space with variations in main-injection duration, post-injection duration, and dwell between the two injections; we also varied load and EGR level. In this study, we have chosen two operating points: one where

the post-injection is most effective for reducing soot at 18% intake oxygen for a given main-injection duration, and one that is the corresponding main-injection-only case.

For the optical diagnostics, we applied soot-PLII at multiple elevations from the firedeck to provide data about both the horizontal and vertical displacements of the soot from the main and post injections throughout the cycle. The soot-PLII data are acquired in one plane at a time, and are phase resolved. In the ensemble, this dataset provides much more spatially and temporally resolved data than our previous experiments and many of those like it. This multi-plane view of the soot field has provided us with more concrete evidence about the mechanism by which post injections reduce soot.

Simultaneously with the acquisition of soot-PLII data, we also used high-speed cinematography to observe the temporal evolution of soot-NL. The high frame rate available with the soot-NL technique provides evidence of the temporal evolution of soot structures in a single cycle that is not available from phase-resolved soot-PLII data. However, the soot-NL technique suffers from several limitations, including a signal bias to hotter soot and, in particular, a lack of spatial resolution along the line of sight. That is, the soot-NL images are two-dimensional projections of complex three-dimensional soot distributions. Hence, it is difficult from the soot-NL data alone to determine if soot structures are merging together, or passing over or under each other from the perspective of the camera. This of course makes it even more difficult to understand the nature of the interaction between the post injection and the main-injection soot. Our recent work [32, 37] made some steps toward interpreting soot-NL data and providing information about the nature of the interaction between the post injection and main-injection soot. In the current study, the multi-plane soot-PLII technique provides information about soot distribution along the soot-NL line of sight so that the two-dimensional projection issues can be more fully resolved. Furthermore, the soot-PLII technique is nearly insensitive to the combustion-heated soot temperature, so comparisons of images from the two techniques also help to resolve the potential temperature bias in soot-NL images. These optical data will also serve well for validation of and comparison with modeling efforts. For more details on the first phase of this multi-year companion modeling effort, see Hessel *et al.* [38].

The remainder of this paper is organized as follows. First is an overview of the experimental facility with a detailed discussion of the soot-NL and soot-PLII diagnostics. Next, the engine-out emissions data at the conditions of interest are summarized, along with a discussion of the high-speed soot-NL images. The soot-PLII images are presented next, and are compared to the soot-NL images. Finally, the important findings and possible next steps are reviewed.

Table 1. Optical engine and fuel system specifications.

Engine base type	Cummins N-14, DI diesel
Number of cylinders	1
Cycle	4-stroke
Number of intake valves	2
Number of exhaust valves	1*
Intake valve opening	703 CAD‡
Intake valve closing	195 CAD‡
Exhaust valve opening	485 CAD‡
Exhaust valve closing	27 CAD‡
Combustion chamber	Quiescent, direct injection
Swirl ratio	0.5 (approx.)
Bore	139.7 mm [5.5 in]
Stroke	152.4 mm [6.0 in]
Bowl width	97.8 mm [3.85 in]
Displacement	2.34 liters [142 in^3]
Connecting rod length	304.8 mm [12.0 in]
Piston pin offset	None
Geometric compression ratio	11.2:1
Replicated compression ratio	16:1
Fuel Injector	Delphi DFI-1.5 (light duty)
Fuel injector type	Common-rail, solenoid actuated
Cup (tip) type	Mini-sac
Number of holes & arrangement	8, equally-spaced
Spray pattern included angle	156°
Nominal orifice diameter	0.131 mm

*In this optically accessible diesel engine, one of the two exhaust valves of the production cylinder head was replaced by a window and periscope (see Fig. 1).
‡All valve timings correspond to the crank angle of the first detectable movement from fully closed.

EXPERIMENTAL SETUP

Optical Engine Experiment

The optical engine is a single-cylinder version of the heavy-duty diesel Cummins N-series (139.7/152.4 mm bore/stroke). The engine is equipped with a Bowditch piston with a right-cylindrical bowl and a flat piston-crown window providing imaging access to the bowl, viewing from below. A flat, round window is also installed in place of one of the exhaust valves for imaging access to a portion of the squish region above the piston (view not used in the current study). A 30-mm wide curved window matching the contour of the bowl-wall allows laser access into the bowl. Flat rectangular windows installed in a ring at the top of the cylinder provide additional laser access through the cylinder wall. Information about engine geometry is in Table 1 and a schematic of the experiment is in Fig. 1. Further details about this engine can be found in Refs. [39, 40].

The fuel is n-heptane, which was selected for its low fluorescence upon illumination by ultraviolet (UV) laser-light. In optical engine studies that use laser diagnostics, n-heptane is commonly used as an approximation for diesel fuels; compared to U.S. diesel fuel, its cetane number of 56 [41] is slightly higher than the value of 44 typical of U.S. diesel fuel [42], a lower density, a much lower boiling point, and zero aromatics. With only a slightly higher cetane number, the autoignition characteristics of these two fuels are similar. The lower boiling point means that the liquid-to-vapor transition in the fuel jet will occur sooner. While the absence of aromatics will affect soot formation, the general in-cylinder mechanisms of post-injection interactions with in-cylinder soot formation and oxidation should be similar [43].

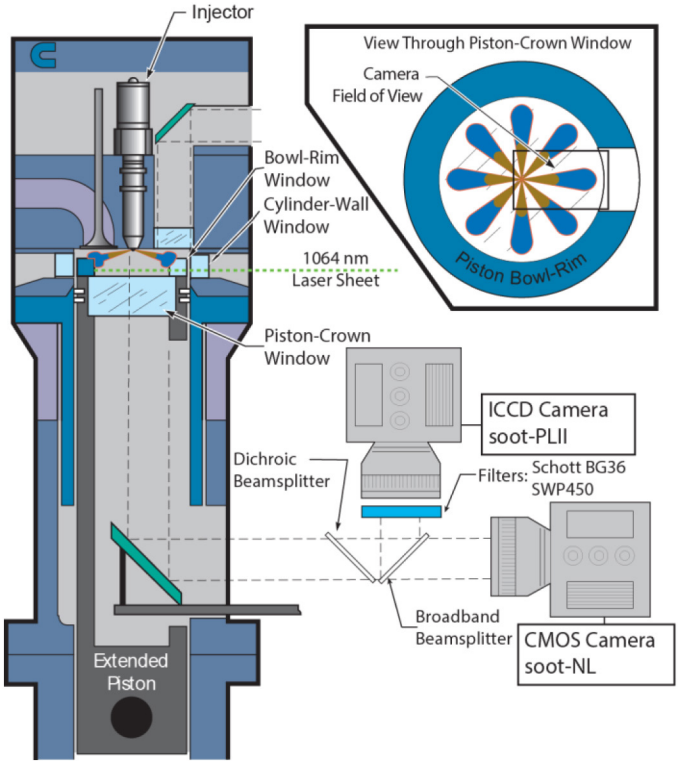

Figure 1. Experimental setup of the single-cylinder engine, laser configuration, and two-camera optical system. The camera field-of-view is shown in the upper right.

The injector is a centrally mounted solenoid-actuated common-rail Delphi DFI 1.5 with eight 131-micron orifices, equally spaced with an included angle of 156°. The heavy-duty injector used in previous studies was replaced by this light-duty injector for its fast response time and its ability to deliver close-coupled, short-duration post injections over a range of injection schedules. Because of the low lubricity and low viscosity of special fuels (such as n-heptane) selected for optical research, the production common-rail fuel pump could not be utilized. Instead, a custom high-pressure diaphragm pump specially designed for low-lubricity fuels pressurizes the fuel rail at up to 2000 bar. The delivery rate of the diaphragm pump is limited, however, and as a result it could only sustainably pressurize the fuel rail to 1200 bar at the static back-leak rate of this particular injector.

Engine Diagnostics

Measurements of cylinder pressure, rate of fuel injection, and engine-out emissions, along with two simultaneous imaging diagnostics, provide data to better understand the mechanism of soot reduction with post injections. Cylinder pressure was measured with an AVL QC34D pressure transducer with a one-quarter crank angle degree (CAD) resolution. The apparent heat release rate (AHRR) was calculated from the measured cylinder pressure using standard techniques [44].

The rate of fuel injection for the two operating conditions was derived from spray momentum measurements. Spray impingement (momentum) was measured by a Kistler 9215 force transducer connected to a Kistler 5004 charge amplifier. Data for each injection schedule were collected at 140 kHz over the span of 200 injections in a collection unit at atmospheric back-pressure [45]. The mass rate-of-injection profiles were derived from the momentum data [46]. The profiles were ensemble averaged and low-pass filtered (Gaussian roll-off at 10 kHz) to remove ringing at the natural frequency of the transducer assembly. While this filtering technique is effective to remove the high-frequency resonance at the natural frequency of the detector, it does introduce small filtering artifacts, such as apparent ringing ahead of the start of injection (also see Fig. 3, discussed later). For more details in the injection rate measurements and injector dynamics, see O'Connor and Musculus [32].

Fuel rate of injection measurements were obtained to measure start of injection and ignition delay timing, but were not used to calculate fuel consumption. In this single-cylinder engine where runs are skip fired and run times are very short, the uncertainties of fuel delivery per cycle are too great to calculate a meaningful fuel consumption metric or measure the effect of post injections on fuel consumption. Some studies have noted that post injections can reduce fuel consumption [5], a possible result of “accelerated combustion” from the post injection [30], although more evidence is needed to understand this mechanism further.

Engine-out smoke was measured using an AVL 415S smoke meter. This device draws a known sample volume of engine exhaust through a filter and measures the change in reflectance (blackening) of the white filter due to accumulated smoke. One potential concern about smoke meter measurements is the response of the meter to adsorbed hydrocarbons. For some LTC conditions that have high adsorbed hydrocarbons, the filter can become tinted with color [47, 48], which could conceivably bias the reflectivity measurement. However, comparisons with other soot and adsorbed hydrocarbon measurement techniques show that even with adsorbed hydrocarbons, the reflectivity strongly correlates with the elemental carbon [47]. Furthermore, no color tinting by adsorbed hydrocarbons is discernible from visual inspection of the loaded filter paper from the current study. Hence, we expect that the reflectivity measurements in the current study are indicative of elemental carbon (C), which

is treated here as synonymous with engine-out soot. We have discussed the use of filter-paper methods for measurement of elemental carbon in this engine in previous works [32].

In this work, we report engine-out soot in milligrams of carbon per cubic meter, which is derived from a correlation computation as follows. The smoke meter quantifies the change in reflectance for a given volume of sample gas as a filter smoke number (FSN) [49]. In this study, FSN was then converted to elemental carbon volume-fraction using a standard correlation from AVL [49]. In each test, sampling commenced before the first fired cycle and continued well after the last fired cycle so that all the exhaust soot for each run was sampled; this amounted to a sampling time of 65 seconds, or approximately 12000 ml of exhaust gas. Although the engine was skip fired, all data reported in this paper have been corrected to the value that would have been measured for continuously fired operation (as if the engine were not skip-fired) by correcting for the intake volume to the smoke meter, referred to as the “effective length” in the AVL calculations. The actual effective length was multiplied by a factor of the ratio of fired time to sample time, where sample time is 65 seconds and fired time is the number of fired cycles divided by engine cycles per second [50]. Repeatability of this measurement was tested at several injection schedules; the standard deviation of the carbon volume-fraction measurements at each of these repeated conditions was approximately 0.05 mg/m^3.

Two complementary imaging techniques were used simultaneously: high-speed natural luminosity imaging and phase-resolved planar laser-induced incandescence of soot. The two techniques shared the same perspective, viewing through the piston-crown window as shown in Fig. 1. A dichroic beam splitter with a cutoff near 485 nm spectrally separated light emitted from the combustion chamber, with long-wavelength light directed to the soot natural-luminosity imaging system, and short-wavelength light directed to the laser-induced-incandescence imaging system. These two techniques, and some of the nuances of using them together, are discussed below.

High-Speed Natural Luminosity Imaging (Soot-NL)

A high-speed (high frame-rate) Phantom 7.1 complementary metal oxide semiconductor (CMOS) camera equipped with a Nikon 105-mm focal-length, f/2.8 glass lens imaged the soot-NL. Previous optical engine studies at similar conditions have shown that soot luminosity is several times brighter than any other source of light during combustion; as a result, we expect that the light from this imaging technique represents soot [46, 51]. The lens aperture was set to f/11. Images with a resolution of 256 × 512 pixels were acquired at half crank-angle intervals (70 microseconds at 1200 RPM). The exposure time was 2 microseconds. The high-speed imaging allows for high frame rates over a long data set; in this study, the entire combustion event during each fired cycle was imaged using this technique.

Planar Laser-Induced Incandescence of Soot (Soot-PLII)

The fundamental output (1064 nm) of a Spectra-Physics Quanta-Ray single-cavity Nd:YAG laser was attenuated to 130 mJ/pulse and formed into a 30-mm wide, approximately 1-mm thick sheet for planar laser-induced incandescence of soot within the engine cylinder. As described in the Optical Engine Experiment section, the sheet was oriented to probe soot horizontally across the width of the bowl, parallel to the firedeck. Using the fundamental output at 1064 nm avoids fluorescence of large poly-cyclic aromatic hydrocarbons (PAH) species, so that only solid soot particles are imaged [52].

As described in previous studies [40], the laser-heated soot emits more strongly at shorter wavelengths than the cooler combustion-heated soot, so the soot-PLII emission was spectrally filtered to shorter wavelengths to improve the signal-to noise ratio of laser-heated to combustion-heated soot. Soot-PLII emission was imaged with an intensified Princeton Instruments PI-MAX 3 camera with a resolution of 1024×1024, a gate time of 15 ns, and at 50% of maximum gain. Two filters, Schott BG36 and SWP450, rejected emission at wavelengths longer than approximately 450 nm. PLII data were limited to one frame per cycle, due to repetition-rate constraints of both the laser and camera systems.

A schematic of the laser imaging planes is provided in Fig. 2. The soot-PLII data were collected along four horizontal planes. One plane elevation was utilized for each engine run, and the sheet elevation was adjusted between runs (the laser sheets were not simultaneous). For each run, the laser sheet was oriented at either 9, 11.5, 14, or 19 mm below the firedeck. The distances from the firedeck were constrained by physical aspects of the engine across the range of crank angles of interest. An elevation 9 mm below the firedeck was the highest sheet position accessible, as constrained by the upper side of the cylinder-wall window. At all heights and at all crank angles, the laser must not be obstructed by the upper surface of the bowl-rim window; this also limited the achievable range of sheet elevations and image crank-angle timings. Note that the position of the piston with respect to these planes changed at each crank angle, but the position of each plane with respect to the firedeck was fixed across all crank angles. For more details on the position of the sheets relative to the piston throughout the range of image acquisition, see Fig. A1 in the Appendix.

The horizontal laser sheet at a given elevation entered from the right of the schematic in Fig. 2, passing through both the cylinder-wall window and the bowl-rim window. While the cylinder-wall window is not curved, the bowl-rim window is curved, with concentric surfaces, so that it is a negative cylindrical lens. Hence, when the laser sheet passes through the bowl-rim window, its divergence in the horizontal plane increases somewhat. Also, the laser sheets were oriented parallel to the firedeck, while the nominal jet axis is declined 12° from the firedeck. Hence, the sheet intersected the jet at a

12 degree angle relative to the jet axis (see Fig. 2) so that the soot-PLII images are not on a nominal symmetry plane of the jet.

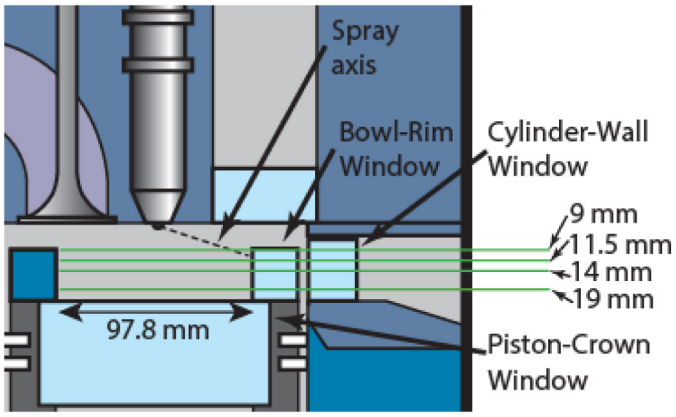

Figure 2. Schematic of four soot-PLII imaging planes at 9, 11.5, 14, and 19 mm from the firedeck.

At each vertical location in the engine and at each crank angle of interest, 40 images were acquired from 40 different cycles to form the ensemble average. Visual inspection of the soot-PLII images shows no significant signal attenuation due to soot deposited on the piston crown window in the first 40 fired cycles. Signal attenuation becomes apparent after 40 fired cycles, so the engine was stopped and windows were cleaned after every 40 cycles. The instantaneous images in each set presented here are from the early cycles of several engine runs. Even though soot accumulation on the piston-crown window could affect the signal collection, soot deposits did not affect the signal creation through laser-induced incandescence - the laser fluence was high enough to ablate nearly all of the soot deposits on the cylinder-wall and bowl-rim windows between fired cycles.

Finally, the instantaneous images shown in this paper are statistically and objectively the “most representative” of the ensemble; to select the most representative image, each image was correlated with every other image in the ensemble, and the image with the highest average correlation coefficient was chosen as the most representative. For more discussion of this image selection technique, see the Ph.D. dissertation by Genzale [36].

Engine Operating Conditions

Table 2 provides an overview of the engine operating conditions. The intake pressure and temperature are elevated from what they would be for a production engine to account for the low compression ratio of the optical engine. While the production engine has a compression ratio of approximately 16:1, the compression ratio of the optical engine is only 11.22:1. The compression ratio is lower in the optical engine primarily because of an increased squish-volume due to the absence of valve pockets in the top of the piston, the absence of the central pip in the piston, an increased ring land crevice, and increased crevices from the flat cylinder-wall windows that do not match the contour of the cylinder bore. To compensate for the lower compression ratio, the engine was operated to replicate the thermodynamic state at top-dead center (TDC) of the piston stroke for a 16:1 compression ratio engine by using a preheated, boosted intake stream [39]. Additionally, this engine was run in skip-fired mode; for every ten cycles, nine were motored using a dynamometer and one was fired. This was done to reduce thermal loads on the optical components.

Table 2. Engine operating conditions.

Engine Speed	1200 RPM
Main-Injection-Only Engine Load	405 kPa gIMEP†
Main- Plus Post-Injection Engine Load	523 kPa gIMEP
Intake O_2	18%
Equivalent EGR	25%
Fuel Pressure	1200 bar
TDC Motored Density	16.6 kg/m^3
TDC Motored Temperature	900 K
Intake Pressure	161 kPa
Intake Temperature	108° C
(16:1 Compression Ratio BDC Pressure)	(99 kPa abs)
(16:1 Compression Ratio BDC Temperature)	(41° C)
Commanded Main Start of Injection ($SOI1_C$)	347 CAD
Actual Main Start of Injection	350 CAD
Commanded Main Duration of Injection ($DOI1_C$)	1550 microseconds
Actual Main Duration of Injection	13 °CA
Main-Injection Fuel Quantity	57.3 mg/injection
Commanded Post Start of Injection ($SOI2_C$)	366 CAD
Actual Post Start of Injection	369 CAD
Commanded Post Duration of Injection ($DOI2_C$)	500 microseconds
Actual Post Duration of Injection	3.5 °CA
Post-Injection Fuel Quantity	13.8 mg/injection

†gIMEP = Gross Indicated Mean Effective Pressure, calculated using indicated work done during compression and expansion strokes only.

The operating condition is typical for modern low-load heavy-duty diesel operation - 18% intake-oxygen, 523 kPa gross indicated mean effective pressure (gIMEP), and a speed of 1200 RPM. The choice of 18% for the intake-oxygen fraction was guided by industry practice with regard to EGR levels commonly used to meet emissions regulations. 18% O_2 was chosen because the corresponding range of EGR (20-30%) is commonly used to meet 2010 US on-road heavy-duty diesel-engine particulate and NO_x regulations [52] with the use of both urea-based selective catalytic reduction (SCR) and diesel particulate filter (DPF) after-treatment systems [3].

The selected post-injection schedule is the minimum-soot condition from previous work [32] with a main- plus post-injection schedule at a main-injection command duration of 1550 microseconds. As will be shown later in the discussion of Fig. 4, we chose this point from a sweep in the post-injection

duration where the *main-injection duration is held constant throughout the post-injection duration sweep*. This kind of test was done intentionally so that with each different post-injection duration, even though the load is not held constant, the conditions of the main-injection would stay the same, creating a constant in-cylinder "initial condition" for the post-injection tests. A more detailed discussion of this experimental design approach can be found in our previous work [32, 37].

RESULTS

Operating Point Characterization

The measured cylinder pressure, rate of injection, and AHRR for both the main-injection-only and the main- plus post-injection operating conditions are in Fig. 3. For both conditions, the AHRR profile contains the characteristic premixed combustion spike (from the start of combustion near 354 CAD to about 360 CAD) followed by a longer mixing-controlled combustion period (starting near 360 CAD). In the main- plus post-injection schedule test, combustion from the post injection is manifest during the mixing-controlled combustion portion as an additional rise in AHRR starting near 370 CAD. The AHRR and injection-rate measurements in Fig. 3 show three important aspects of the ignition delays and combustion characteristics for the two injections.

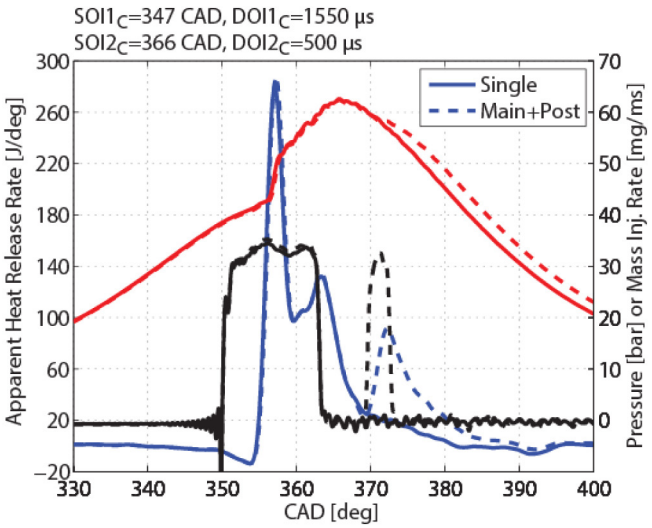

Figure 3. Cylinder pressure (red), rate of fuel injection (black), and AHRR (blue), for main-injection operation (solid) with $SOI1_C$=347 CAD and $DOI1_C$=1550 microseconds; and main- plus post-injection operation (dashed) with $SOI1_C$=347 CAD, $DOI1_C$=1550 microseconds, $SOI2_C$=366 CAD, and $DOI2_C$=500 microseconds.

First, the actual main-injection duration is 13 °CA, while the main ignition delay is only approximately 4 °CA. As a result, the ignition dwell for the main injection, from the end of the main injection near 363 CAD, to the start of main combustion near 354 CAD, is negative. A negative ignition dwell is typical for conventional diesel conditions. (Advanced low-temperature combustion modes, by contrast, typically have a positive ignition dwell). Second, the relatively low level of the mixing-controlled AHRR peak compared to the premixed burn peak is typical of a low-load condition. Much of the fuel from the main injection is consumed in the premixed burn, but the relatively short main-injection duration means that the net heat release from mixing-controlled combustion is relatively small compared to higher-load conditions.

Third, the ignition delay of the post injection is only 1 °CA, which is much shorter than the main injection ignition delay (4 °CA). This difference is likely driven by the higher in-cylinder ambient density and local temperatures encountered by the post-injection fuel. With such a short ignition delay, the post-injection combustion does not exhibit the same two-stage burning characteristics of the main injection, but instead burns as a single heat-release event. The relatively short post-injection ignition-delay does not provide as much time for fuel/air premixing before ignition, meaning that combustion of the post-injection fuel should be more mixing-controlled.

Engine-Out Soot Measurements

Engine-out soot measurements for both a single-injection duration sweep and a main- plus post-injection sweep are shown in Fig. 4. These data were obtained through two separate sets of tests. The single-injection baseline (closed squares) was collected by varying the commanded duration of the single injection ($DOI1_C$) from 1350 to 2750 microseconds, corresponding to engine loads from 350 to 750 kPa gIMEP, while holding the command start of the single injection ($SOI1_C$) constant at 347 CAD. For the post-injection sweep (open symbols), a post injection of increasing commanded duration ($DOI2_C$) from 300 to 1200 microseconds was added to one main-injection duration, $DOI1_C$=1550 microseconds. The commanded start of injection for the post injection ($SOI2_C$) was held constant at 366 CAD.¥

The engine-out soot data in Fig. 4 clearly show that the post injection reduces engine-out soot compared to a single injection at the same load over a wide range of post-injection durations, from $DOI2_C$=300 microseconds to 800 microseconds. At the condition considered in this paper, $DOI2_C$=500 microseconds, the post injection reduces engine-out soot by 40% compared to a single injection at the same load of 523 kPa gIMEP. At longer post-injection durations, the engine-out soot at a given load is lower than for a single injection at the same load, but the magnitude of the post-injection soot reduction decreases as the post injection duration increases. Eventually, the engine-out soot with a long post-injection is larger than for a single injection at the same load. For this particular condition, the cross-over point, where the addition of a post injection is detrimental to engine-out soot

¥. Compared to previous data [32] at the same injector command conditions, the absolute magnitudes of both the loads and exhaust soot are slightly different. For example, the load at the $DOI1_C$=1550 microseconds, $DOI2_C$=500 microseconds condition is approximately 7% higher than in the previous tests. The difference is most likely due to slight changes in injector performance as the new injector "breaks in." Even with the slight differences in an absolute sense, the trends are the same as data from previous tests at the same conditions, and the emissions data at a given load are nearly identical.

as compared to a single injection at the same load, is at approximately a $DOI2_C$=900 microseconds and 670 kPa gIMEP.

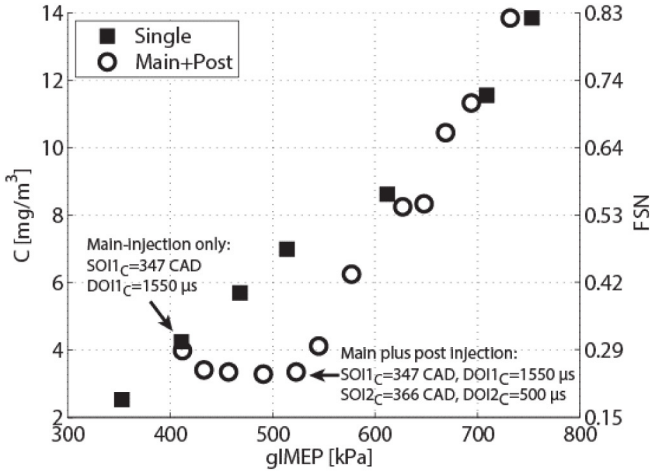

Figure 4. Filled squares: engine-out soot levels for a single-injection sweep with $SOI1_C$=347 CAD and $DOI1_C$=1350-2750 microseconds. Open circles: main injection with $SOI1_C$ = 347 CAD and $DOI1_C$=1550 microseconds with post injections added at $SOI2_C$=366 CAD and $DOI2_C$=300-1200 microseconds.

Furthermore, and quite importantly, Fig. 4 conclusively shows that the post injection must be interacting with the main-injection in-cylinder soot to reduce the engine-out soot over a range of $DOI2_C$=300 microseconds to 550 microseconds. This is evident by comparing the engine-out soot level of the main- plus post-injection operation with that of the lower-load single injection condition with the same duration as the main-injection (i.e., the "main-injection-only" condition).* That is, the engine-out soot with only the main-injection at $DOI1_C$=1550 microseconds (411 kPa gIMEP) is 4.25 mg/m^3, while the engine-out soot at the main- plus post-injection condition with $DOI1_C$=1550 microseconds and $DOI2_C$=500 microseconds (532 kPa gIMEP) is 3.35 mg/m^3, 20% lower than with just the main injection. This comparison is important because it clearly shows that with an unchanged main injection, the post injection *must be* interacting in some way with the in-cylinder main-injection soot to reduce the engine-out soot.

Recalling the three proposed soot-reduction mechanisms described in the introduction, this result indicates that the mechanism for engine-out soot reduction for these data cannot be solely the injection-duration effect; the reduction in soot must also stem from a fluid mechanical or thermal interaction between the post injection and the main-injection mixture. At post-injection durations greater than $DOI2_C$=550 microseconds, it is still very likely that the post jet interacts with the main-injection products, but as discussed in O'Connor and Musculus [37], the additional soot likely created by the post injection itself increasingly outweighs the soot reduction resulting from the interaction of the post jet with the main-injection mixture.

Understanding more about the nature of this interaction is the goal of the current study. Our earlier work [37] began to explore the interaction process, but the soot-PLII data were only obtained in one plane, resulting in limited information about the spatial distribution of soot in the combustion chamber. In the next section, we discuss the results of the simultaneous soot-NL and multi-plane soot-PLII imaging, from which the development of in-cylinder soot is more clearly revealed.

Soot-NL Imaging

A time series of soot-NL images is shown in Figs. 5a and 5b. In these images, only one of the eight jets from the injector is fully captured. The partial view shows the injector tip on the left and the bowl wall on the right-hand side of the image. The jet of interest propagates horizontally from left to right in the image. In both figures, the leftmost and center columns are ensemble averages of 20 images for the main-injection-only and main-plus post-injection conditions, respectively. The rightmost column shows instantaneous images for the main- plus post-injection condition. The series begins at 370 CAD at the top of Fig. 5a, and progresses downward by rows in 0.5 °CA increments to 372.5 CAD, and continues in Fig. 5b from 373 to 375.5 CAD. As discussed above in reference to Fig. 4, the reduction of engine-out soot compared to the main-injection-only case indicates that there is a substantial interaction between the post jet and the main-injection mixture. The crank angle range presented in Fig. 5 corresponds to the initial interaction of the post jet with the main-injection soot.

The start of the time series at 370 CAD is 1 °CA after the actual start of the post injection (see Fig. 3). At this point in the cycle, the upper right image shows the liquid sprays of the post injection, which are weakly visible by Mie scattering of the soot natural luminosity (combustion heated, no laser yet). No discernible soot luminosity has yet appeared in the post jet, and most of the luminosity signal is due to soot from combustion of the main injection. Two large regions of soot from the main injection are located near the piston bowl-wall (right side of image) on either side of the jet centerline. Prior to this image, the main-injection has already impinged on and spread along the bowl wall. As a result, the main-injection soot resides primarily in two counter-rotating vortical structures on either side of the horizontal jet centerline, as indicated in Fig. 5. Although the rotational motion of the vortical structures is not obvious in the static images of Fig. 5, they are more apparent in dynamic cinematographs of the images, which are provided at [53, 54]. These two vortical structures of soot are formed by the interaction of the horizontal jet with the two adjacent jets on either side of it. Within these soot structures, it is unclear from this line-of-sight technique how the soot is distributed vertically (i.e., in the direction of the cylinder axis, perpendicular to the firedeck).

*. Here, the term "main injection" refers to the first injection of a post injection condition. "Single injection" generally refers to a condition that has the same load as the post-injection condition, but with only one injection, such that the single injection is longer than the main injection of the post-injection condition.

After its initial appearance at 370.5 CAD, soot luminosity in the post jet increases significantly just 0.5 °CA later, at 371 CAD, where soot luminosity appears across much of the apparent head of the post jet. Images another 0.5 °CA later show strong soot luminosity distributed across the head of the post jet. This distribution of soot luminosity is consistent with the soot-filled jets described by Dec for conventional diesel combustion [40]. An interaction between the post jet and the main-injection mixture is also first discernible at 371.5 CAD, as annotated in blue, where the head of the post jet interacts with the soot structure on the bottom of the image. Although the annotated interaction is not obvious in these static images, it is more evident from visual inspection of the cinematic sequences of images. Further evidence of this interaction is also much more apparent in the ensemble-averaged soot-PLII images that are discussed later in the paper.

The high-speed cinematograph shows how the interaction develops through the next several crank angles. The cinematic sequence seems to show the head of the post jet "pushing" or displacing the main-injection soot located in the soot structure in the lower part of the image. This explanation would be consistent with the behavior of starting jets, where the jet fluid displaces ambient fluid ahead of it as the jet penetrates through the medium [55]. However, we are unable to verify such displacement from the soot-NL images because the flow field "tracer," in this case soot, is a non-conserved scalar. The apparent displacement could instead be the progressive, rapid oxidation of the main-injection soot structure, creating a moving "front" of oxidation that appears very similar to fluid displacement. (Complementary evidence of this interaction from soot-PLII imaging is presented later, in the discussion of Fig. 7.)

As the post-jet penetrates into/past the region of main-injection soot, the soot luminosity from the post and main injections merges together so that soot from the two injections becomes largely indistinguishable, as notated in 372.5-373.5 CAD in Fig. 5. Due to the line-of-sight limitations of soot-NL imaging, it is unclear whether these two regions are indistinguishable as a result of actual merging of the luminous soot from the main and post injections, or if it is because the two soot distributions are separate but at different vertical elevations along the line of sight. (Evidence from the soot-PLII images presented in the next series of figures indicates that there is actual merging of the post-injection soot with the main-injection soot at these timings.)

Between 374 and 375 CAD, the post jet reaches the bowl wall and thereafter it impinges on the wall, spreading to either side of the jet centerline, much like the main jet before it. At this timing, the post-injection luminous soot appears to merge with that of the main-injection, which is easier to discern in the dynamic cinematic movie than in the static images of Fig. 5. Even though the movie provides some indications of the contributions of main- and post-injection soot to the overall luminosity, it is impossible to definitively discriminate between them from these line-of-sight images. Nevertheless, at the end of the sequence of ensemble-average images, soot luminosity that is apparently from the main injection (bottom of images in lower rows of Fig. 5b) seems to maintain approximately the same intensity with the post injection. This intensity comparison is hindered somewhat by the increase in overall luminous emission from the addition of the post injection, which raises the overall background intensity throughout the image, evidenced for instance in the increased visibility of mechanical features on the firedeck. In the next section, the soot-PLII images reveal, among other things, a much greater contrast between main-injection soot with and without a post injection than is apparent from the soot-NL technique.

Soot-PLII Imaging

To better probe the interaction between the post jet and the main-injection products, we turn to the soot-PLII images for more information. Figures 6, 7, 8, 9 show soot-PLII images from the four laser-sheet planes in Fig. 2 at four key crank angles of the post-injection event. In each of these figures, three sets of images are provided. The left column shows the ensemble-average of 40 images for the main-injection-only. The middle column contains the ensemble-average of 40 images for the main- plus post-injection condition. The right column images are the most representative instantaneous main- plus post-injection images at each location and crank angle (the technique for selecting the "most representative" image is described in the Engine Diagnostics section above). In each image, the crank angle degree and elevation of the laser plane below the firedeck is indicated in the upper left corner.

Like the soot-NL images, soot-PLII images are a partial view of the combustion chamber, focusing on one jet penetrating horizontally from the perspective of the camera. The injector is located on the left, indicated by a white dot, and the bowl wall is on the right, indicated by a white curved line. The jet intersected by the laser sheet penetrates horizontally from left to right, and the laser sheets in these images enter the chamber from the right side of the images. Recall that each horizontal laser sheet intersects the jet at a 12 degree angle relative to the jet axis (see Figs. 2 and A1). Also, as described in the Engine Diagnostics section, the sheet elevation is adjusted between engine runs to generate soot-PLII images from separate cycles but at different planes within the combustion chamber.

Figure 6 shows soot-PLII images in four planes at 370 CAD, before any soot is formed in the post jet. At 370 CAD, which is 1 °CA into the post injection, very weak interference from the liquid jets is visible, especially in the ensemble-averaged post-injection images (middle column). Strictly speaking, it is not possible to quantitatively compare intensities or even relative distribution of intensities due to uncertainties of the soot-PLII technique, which include differential laser attenuation, shot to shot variability in laser pulse energy and/or energy distribution across the laser sheet, and signal trapping [56]. Nevertheless, the similarity of the ensemble-averaged main-injection-only and main- plus post-injection images (left and middle columns) indicates that the post injection has had almost no effect on the main-injection soot at this early timing. This spatial soot distribution acts as an "initial condition" for the approaching post jet.

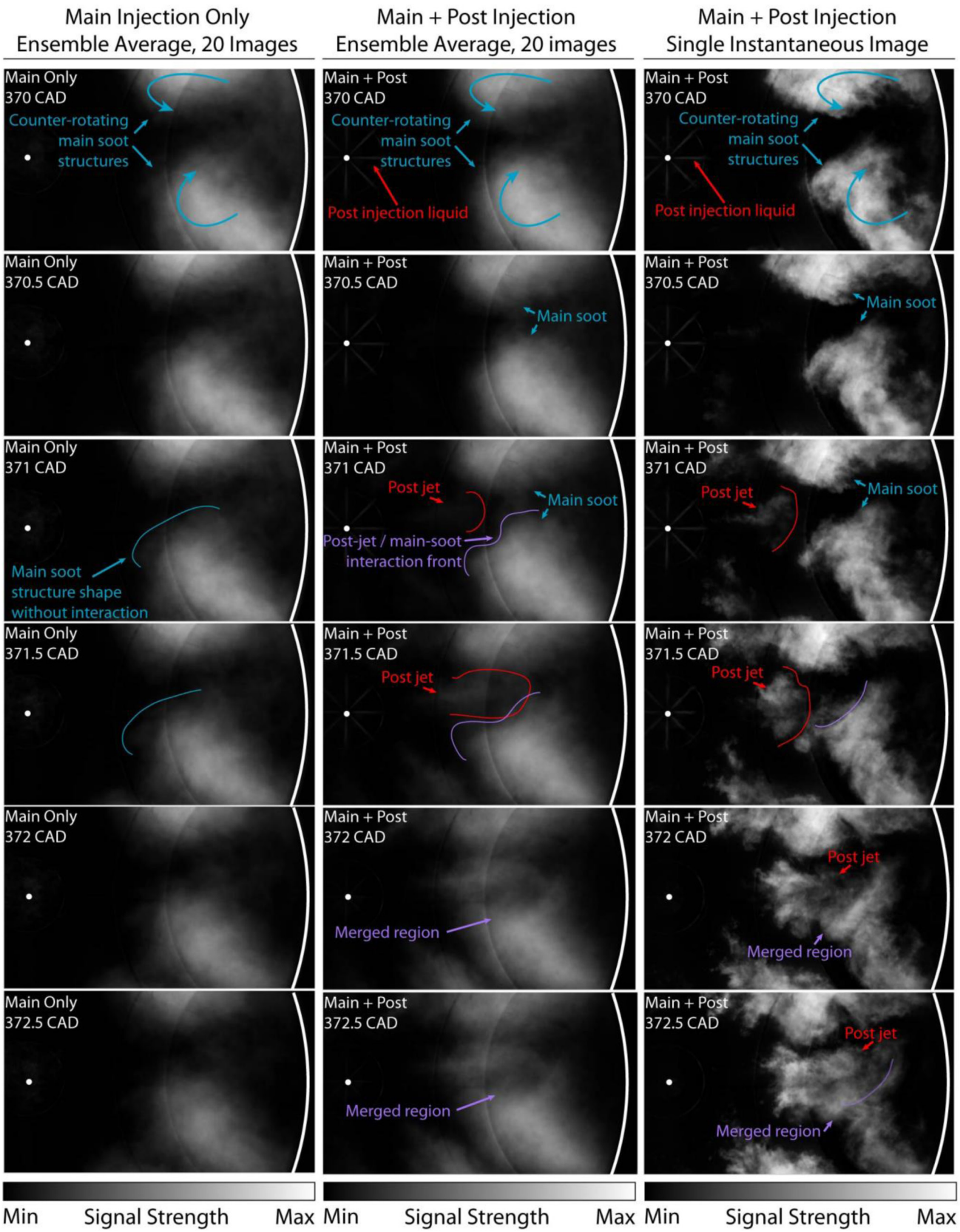

Figure 5a. Time series of instantaneous soot-NL images for conditions with either main injection only (left) or main- plus post-injection (center and right). $SOI1_C$=347 CAD, $DOI1_C$=1550 microseconds, $SOI2_C$=366 CAD and $DOI2_C$=500 microseconds. The white dot at the left indicates the position of the fuel injector and the curved white line on the right represents the piston bowl-wall. Swirl ratio is 0.5 and swirl rotates counter-clockwise.

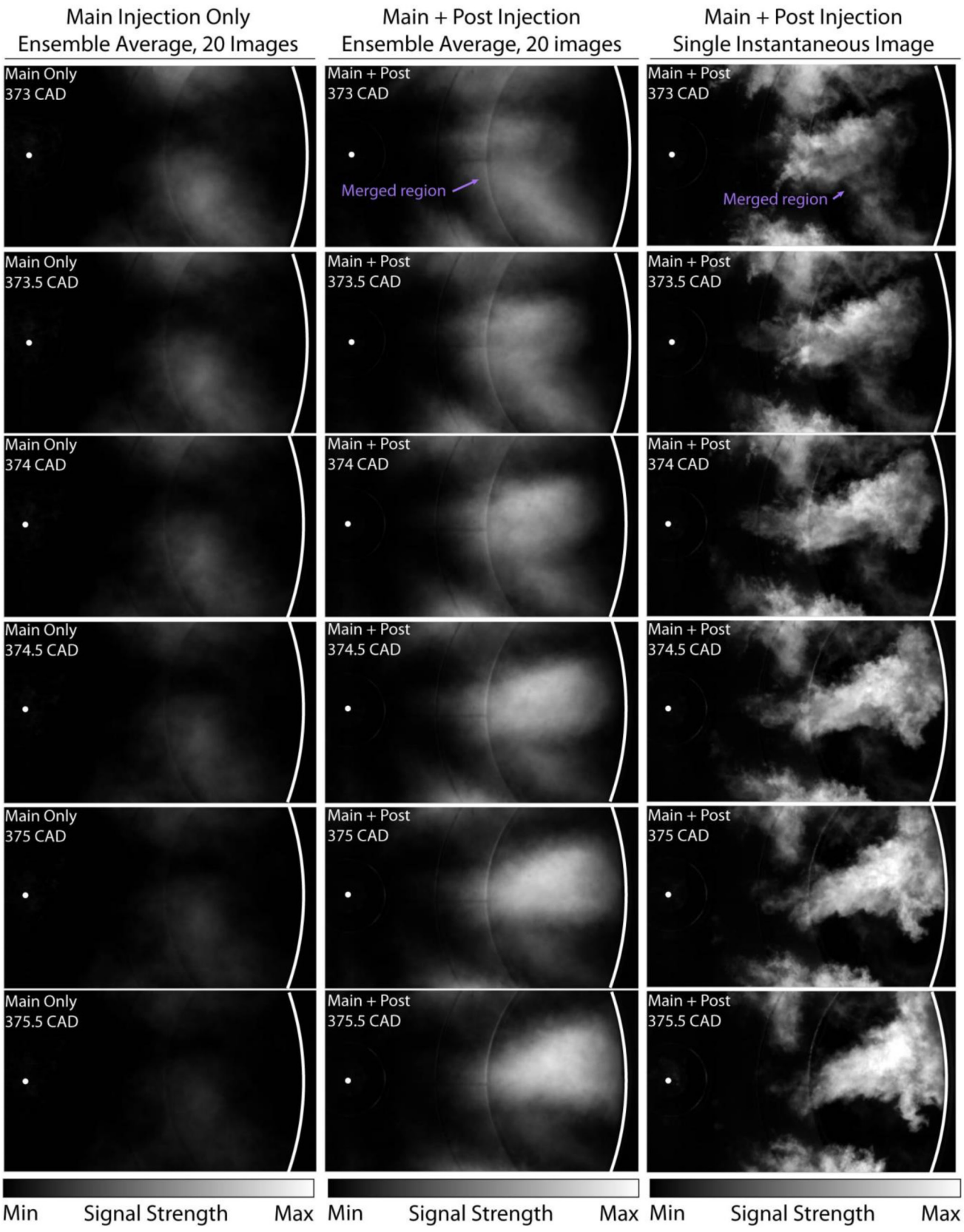

Figure 5b. Time series of instantaneous soot-NL images for conditions with either main injection only (left) or main- plus post-injection (center and right), continuing from Fig. 5a. $SOI1_C$=347 CAD, $DOI1_C$=1550 microseconds, $SOI2_C$=366 CAD and $DOI2_C$=500 microseconds. The white dot at the left indicates the position of the fuel injector and the curved white line on the right represents the piston bowl-wall. Swirl ratio is 0.5 and swirl rotates counter-clockwise.

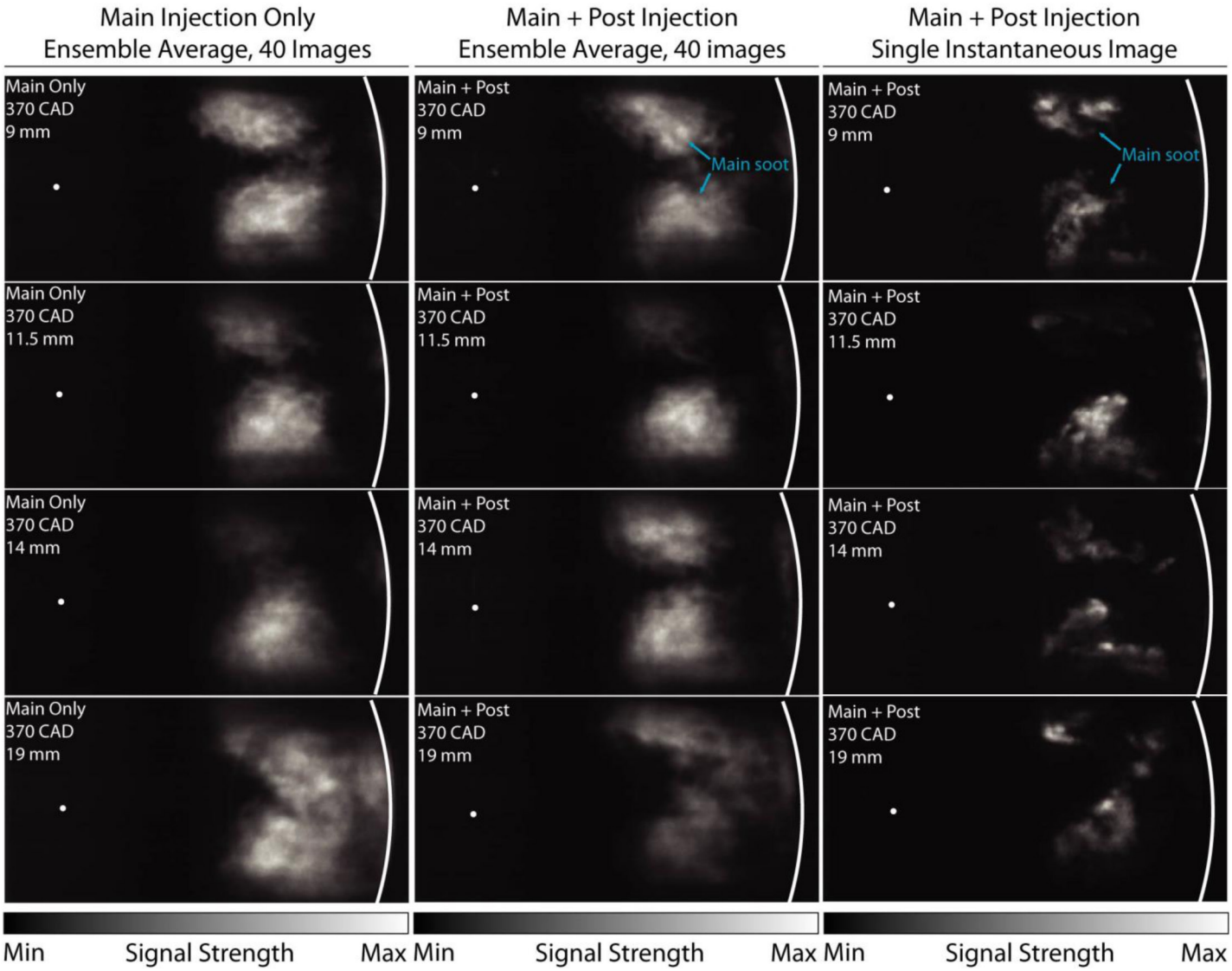

Figure 6. Soot-PLII images at 370 CAD in horizontal planes at four elevations below the firedeck (arranged by rows), as noted on each image. Columns show images ensemble averaged over 40 cycles for main-injection only (left) or for main- plus post-injection (middle), or representative instantaneous images for main-plus post-injection (right). $SOI1_C$=347 CAD, $DOI1_C$=1550 microseconds, $SOI2_C$=366 CAD and $DOI2_C$=500 microseconds. Swirl ratio is 0.5 and swirl rotates counter-clockwise.

Additionally, at this early point in the cycle, the distributions of main-injection soot at all four elevations from the firedeck are similar in shape. Similar to the line-of-sight soot-NL images in Fig. 5, soot structures are located on either side of the jet axis and less soot is found between these structures, especially at the upper elevations. At this particular timing and operating condition, with similar spatial distribution of soot at all elevations in the soot-PLII images, the soot-NL image (at 370 CAD) should be fairly representative of the actual soot distribution throughout the bowl. That is, the gradients in soot volume fraction along the line of sight are small, so the luminosity signal should roughly represent the soot distribution along the whole line of sight. This does not happen everywhere in the cycle, however. Furthermore, temperature gradients along the line of sight bias the soot-NL signal to the soot that is hotter and/or closer to the camera. Unfortunately, information about line-of-sight temperature gradients is not available from either dataset, so the possible effect of a temperature bias in the soot-NL images cannot be assessed. Hence, the soot-NL images may still have significant bias to hot soot due to whatever temperature gradients may exist along the line of sight.

The first interaction of the post-jet with the main-injection soot is apparent in the soot-PLII images at 372 CAD (Fig. 7). As noted earlier in the discussion of the soot-NL images in Fig. 5, the post jet interacts with the soot from the main injection, and soot from the main- and post-injections begins to merge together.

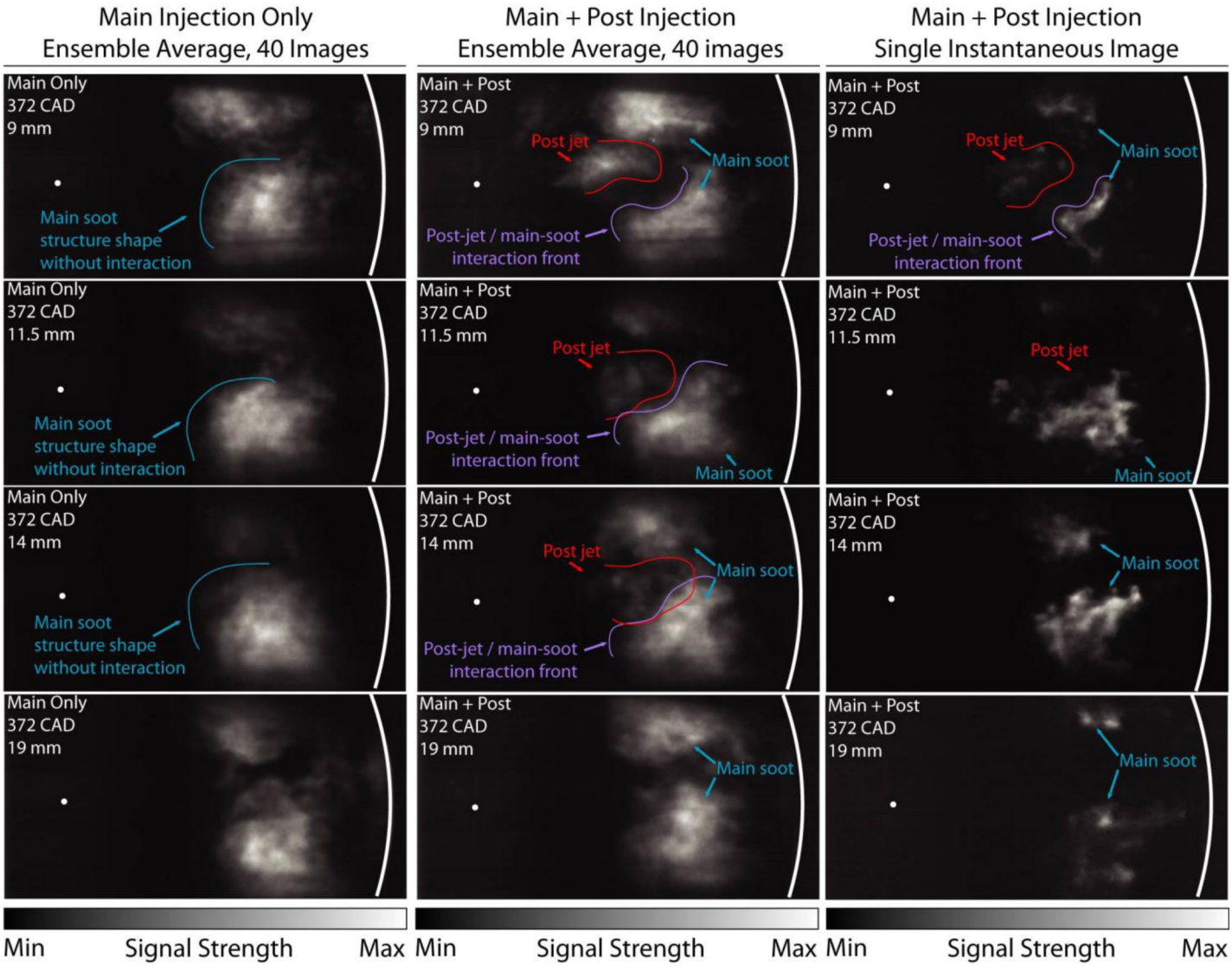

Figure 7. Soot-PLII images at 372 CAD at four horizontal elevations below the firedeck (arranged by rows) with approximate boundaries for the main-injection and post-injection soot. Columns show images ensemble averaged over 40 cycles for main-injection only (left) or for main- plus post-injection (middle), or representative instantaneous images for main-plus post-injection (right). $SOI1_C$=347 CAD, $DOI1_C$=1550 microseconds, $SOI2_C$=366 CAD and $DOI2_C$=500 microseconds. Swirl ratio is 0.5 and swirl rotates counter-clockwise.

Comparison of the main- plus post-injection images with those for only the main injection clearly shows the interaction of the post jet with the main-injection soot in a highly repeatable fashion; this interaction is seen in the instantaneous main- plus post-injection images as well. First, in the images in the top row of Fig. 7, 8, 9 mm from the firedeck), the soot structures in the main-injection-only images are undisturbed and relatively circular. The corresponding soot structures in the main- plus post-injection images, however, have clearly been disturbed by the penetration of the post jet. A large region of soot has been carved from the soot structure near the bottom of the image, either by displacement or oxidation. The fact that this feature is so clearly defined in an ensemble-averaged image indicates that this process is highly repeatable and occurs during most (if not all) cycles. This feature in the main-injection soot structure is also visible in the most-representative instantaneous image; the main-injection soot, indicated by the blue arrows, has been disturbed by the post jet, indicated by the red arrows. Similar features in the main-injection soot structures are visible in the images at 11.5 and 14 mm from the fire deck.

At 372 CAD, the spatial distribution of soot at each elevation is much different than at 370 CAD. Most importantly, the post jet has only penetrated far enough to reach the 9 mm, 11.5 mm, and 14 mm planes; see the nominal jet axis relative to planes in Fig. 2, or for more detail on estimated jet penetration relative to the laser sheet elevations, see the Appendix. In the top two images in Fig. 7, the head of the post-jet appears to penetrate farther in the 11.5 mm image; this is a result of the 12° angle between the horizontal laser plane and the nominal jet axis (see Fig. 2 or A1). According to the penetration calculations for Fig. A1, the head of the post jet should not have reached the 14 mm elevation at 372 CAD; the appearance of soot from the post at 14 mm in the soot-PLII data is likely due to cycle-to-

cycle variation of the jet path and/or widening of the head of the jet, as discussed by Dec [40]. At 372 CAD, soot in the post jet is not yet present in the lowest elevation, 19 mm. In addition, there is little displacement or alteration of the main-injection soot distributions relative to the 19 mm single-injection images in the left column, so the post-jet itself likely has not yet penetrated into this plane.

At the 9-mm elevation at 372 CAD, soot appears in the post-jet (annotated in the figure) in a region that is soot-free with only the main injection. For the most part, the apparent post-injection soot-PLII signal is also spatially separated from the main-injection soot-PLII, so that the post-injection soot is distinct from the main injection soot. Visual inspection of each image in the set confirms that this is the typical instantaneous behavior. By contrast, in the instantaneous image at the 11.5-mm elevation, soot also appears in the post-jet (annotated in the figure) in a spatial location that was soot-free with the main injection only, but it is difficult to discern the post-jet soot from the main-injection soot. Unlike the images at the 9-mm elevation, there is no clear separation between the post-jet and main-injection soot-PLII signals in the instantaneous image, the soot-PLII signals are spatially merged. However, the ensemble-averaged images at 11.5 mm display features that are consistent with frequent separation, as there is a zone of low intensity between the post-jet and main-injection soot. In the main-injection-only images (left column), soot-PLII signals are much stronger in the same spatial location as the separation region in the images with a post injection. These observations provide evidence of the interaction between the post jet and the main-injection soot at this elevation. The same description holds true at the 14 mm elevation as well. However, it is difficult to determine the extent of mixing between the post jet and the main-injection soot, as was discussed above with reference to the soot-NL images in Fig. 5.

Later in the cycle, soot from the post-injection merges with main-injection soot, especially at the middle two elevations. Figure 8 shows soot-PLII images at 373 CAD, when the post jet penetrates past the main-injection soot structures. Further, Fig. 9 shows the point at 375 CAD when the post jet impinges on the bowl wall and begins to spread and merge into the regions of the residual main-injection soot. At 373 CAD, the merging of the post- and main-injection soot makes it difficult to distinguish between the two structures. However, based on the extent of the soot toward the top and bottom of the ensemble-averaged images at this timing, it is clear that two large main-injection soot structures remain at all elevations. These soot structures have been indicated in Fig. 8 with blue arrows. These regions of main-injection soot relate well to those in the single-injection case in the left column. While it is very likely that there is interaction between the post injection and the main-injection soot during this time, we are unable to discern the extent of mixing between the post jet and the main-injection soot from either the ensemble-averaged or instantaneous images.

However, looking now at the 375-CAD images in Fig. 9, after the post jet has impinged on the wall, the apparent main-injection soot, particularly at the lower elevations of 14 mm and 19 mm, is almost gone. To see this clearly, compare the soot-PLII intensities within the annotated ellipses in Fig. 9 of the ensemble-average main-injection-only images (left column) relative to main- plus post-injection images (middle column). In the main-injection-only images, soot structures are present on either side of the jet centerline. In the main- plus post-injection images, this soot is all but gone. Instead, the soot is predominantly along the centerline where the post jet is located. Recall that in the soot-NL images of Fig. 5, the luminosity of the main-injection soot structures remained nearly the same as the post jet impinged on the wall. Because the main-injection soot signal reduction is evident in a soot-LII image, which indicates the location of soot regardless of its combustion-heated temperature, (as opposed to a soot-NL image where the intensity is highly correlated to soot temperature), we can more confidently conclude that interaction between the post jet and the main-injection soot results in a dramatic difference in soot distribution within the laser planes. It is possible that the reduction of soot within the laser planes is due in part to displacement of the soot out of the laser planes, where it is not probed, e.g. between the lowest sheet and the bottom of the piston bowl (see Fig. A1). Alternatively, image analysis in our previous work [37] has suggested that the intensity reduction may be in part due to entrainment of the main-injection soot into the post jet. That is, some of the main-injection soot structure may be pulled into the post jet, leaving less soot in the regions formerly occupied by main-injection soot. Additionally, the signal could have decreased because of lower soot concentrations due to enhanced oxidation. This enhanced oxidation could be a direct effect associated with mixing in the vicinity of the post jet. It may also be a more indirect effect for which the post jet displaces the main-injection soot into a region of higher oxygen concentration and/or higher temperature, thereby increasing the rate of soot oxidation. Of course, the engine-out soot measurements show a reduction with the addition of a post-injection, which is consistent with enhanced oxidation of the main-injection soot.

Further exploring the comparison of signal intensity trends for soot-NL relative to soot-PLII, the stark differences in the ensemble-average soot-PLII signal for the main-injection soot structures with and without a post-injection also suggest that a temperature bias may be significantly affecting the soot-NL signals in Fig. 5. In particular, two features of the ensemble-average images (left two columns) at 375 CAD in Fig. 5b are consistent with a soot temperature bias in the intensity measured by the soot-NL technique. First, as already discussed, the main-injection soot structures have nearly the same signal intensity in the same spatial locations with the addition of a post injection. Increased background interference from reflections of luminosity off the cylinder head in the lower image make this comparison less than straightforward, but relative to the background intensity, the main-injection soot luminosity with the post-injection appears roughly equivalent to

that without the post injection, as already noted for the instantaneous images in Fig. 5b. By contrast, regions of the ensemble-average soot-PLII images are much weaker with a post injection (bottom of middle column in Fig. 9) than without one (bottom left of Fig. 9). In particular, the main-injection soot within the blue ellipses in the left column of Fig. 9 is not present in the post-injection cases in the middle column of Fig. 9, which is most likely a result of redistribution and/or enhanced oxidation of main-injection soot.

Second, the post-injection soot luminosity (center-right of images at 375 CAD in middle column of Fig. 5b) is much stronger than the soot luminosity with the main injection only (left column in Fig. 5b). By contrast, the post-injection soot-PLII signals (middle column of Fig. 9) have roughly the same intensity as the main-injection-only soot (left column of Fig. 9).

The inconsistencies between intensity in the soot-NL images compared to the soot-PLII images may be caused by differences in combustion-heated soot temperature across the images. For instance, if the main-injection soot structures were cooler than the post-injection soot, then the signal from the main injection soot would be much weaker, as is apparent in Fig. 5. Furthermore, with relatively weak luminous intensity for the cooler combustion-heated main-injection soot, the intensity reduction due to greater soot oxidation by the post-injection would be less apparent, given the relatively strong background interference. The soot-PLII technique, for which the laser-heated soot is virtually unaffected by the initial combustion-heated soot temperature, is much less sensitive to these temperature biases. Hence, the above comparisons between soot-NL in Fig. 5 and soot-PLII in Fig. 9 clearly illustrate that soot-NL images must be interpreted with care.

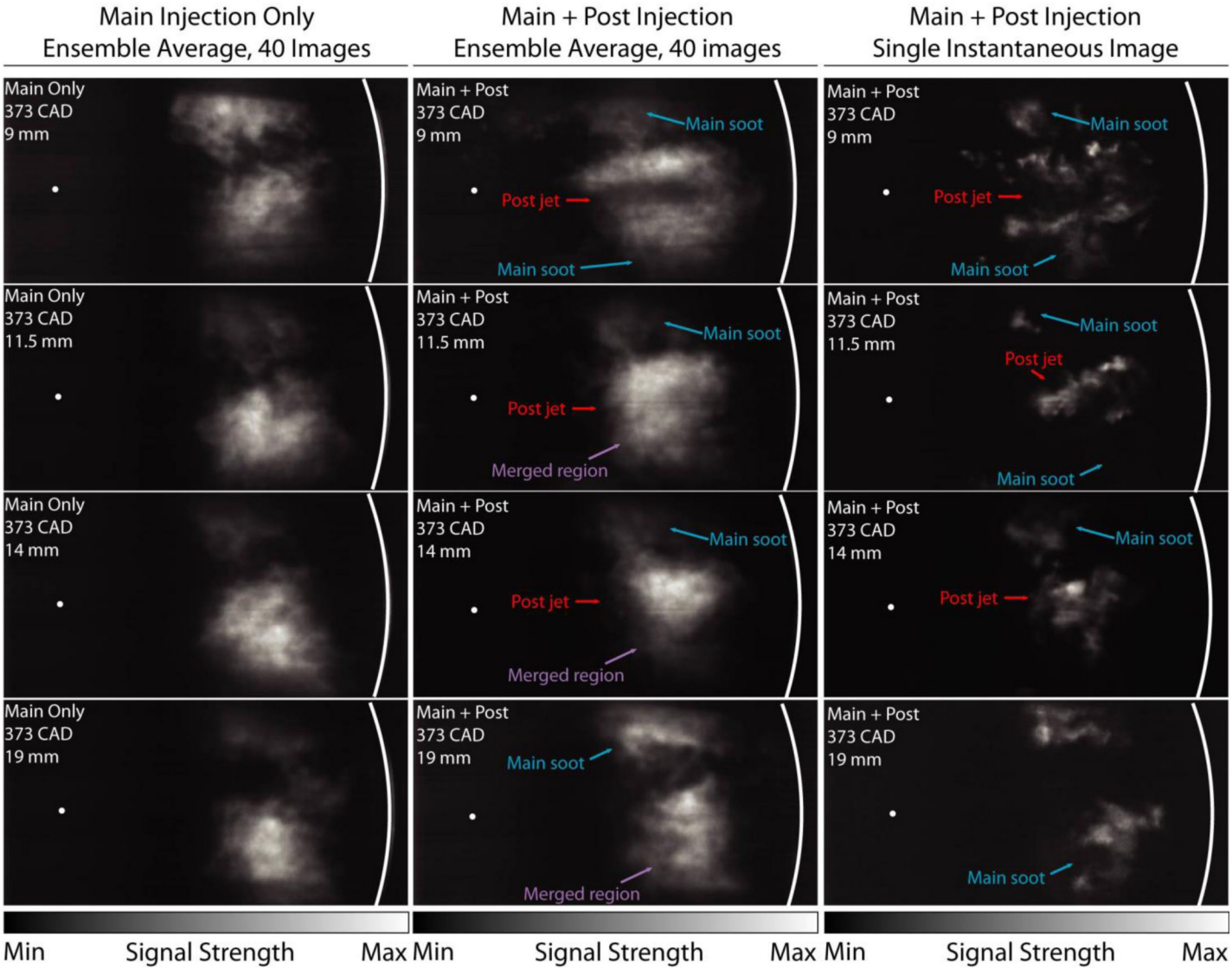

Figure 8. Soot-PLII images at 373 CAD at four horizontal elevations below the firedeck (arranged by rows). Columns show images ensemble averaged over 40 cycles for main-injection only (left) or for main- plus post-injection (middle), or representative instantaneous images for main-plus post-injection (right). $SOI1_C$=347 CAD, $DOI1_C$=1550 microseconds, $SOI2_C$=366 CAD and $DOI2_C$=500 microseconds. Swirl ratio is 0.5 and swirl rotates counter-clockwise.

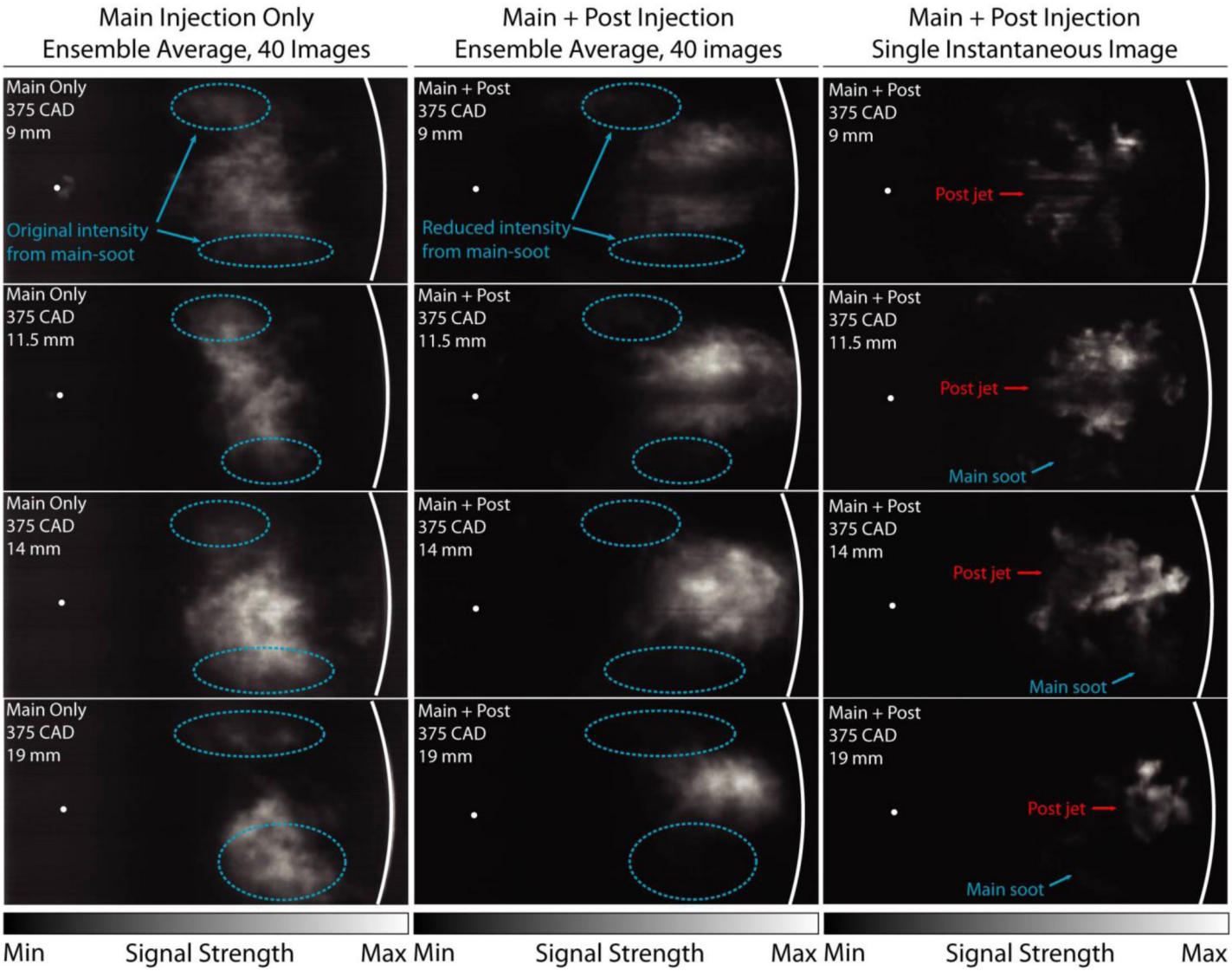

Figure 9. Soot-PLII images at 375 CAD in horizontal planes at four different elevations below the firedeck (arranged by rows), as noted on each image. Columns show images ensemble averaged over 40 cycles for main-injection only (left) or for main- plus post-injection (middle), or representative instantaneous images for main-plus post-injection (right). $SOI1_C$=347 CAD, $DOI1_C$=1550 microseconds, $SOI2_C$=366 CAD and $DOI2_C$=500 microseconds. Swirl ratio is 0.5 and swirl rotates counter-clockwise.

One other example where caution must be exercised in the interpretation of soot-NL images is in the full series of images throughout the combustion event as presented in the soot-NL cinematographs [53, 54]. In the combined cinematograph, which extends beyond the 375-CAD end of the static images presented here, the combustion luminosity for the post-injection condition extends much later into the cycle than with the main injection only. Without considering the influence of temperature on the natural luminosity intensity, the increased late-cycle soot luminosity might suggest that a post-injection would increase engine-out soot. The direct measurements of engine-out soot of course show the opposite. Hence, in this example, trends in late-cycle soot luminosity are counter to trends in the eventual soot emissions at the end of the cycle.

Clearly, changes in intensity of soot luminosity can be due to changes in the amount of soot, but they can also be due to changes in temperature. Discriminating between the two effects is not straightforwad without some other independent measurement, such as soot-PLII in multiple planes as employed here.

SUMMARY

Returning to the three general mechanisms that have been proposed to explain how post injections reduce soot, the results of this study clearly show that interaction between the post jet and the main-injection in-cylinder soot is driving the reduction of the engine-out soot. The engine-out soot trends in Fig. 4 show that the post-injection must interact with the residual main injection soot, and the soot-NL and soot-PLII images show that this interaction involves displacement and/or

oxidation in some regions, and merging of post- and main-injection soot in other regions or at other times. As discussed above, this means that the "duration-driven" explanation of soot reduction, which does not account for interactions between injections, cannot fully explain the reduction in soot. Furthermore, the merging of post- and main-injection soot observed in the soot-PLII data show that a "split flame," for which the post injection burns separately from the main injection, is not observed, and hence is not essential for soot reduction. However, the results of this study cannot rule out either the mixing-driven or temperature-driven explanations. Several observations do however suggest that the mixing-driven explanation may involve multiple mechanisms, including both a direct mixing enhancement in the vicinity of the post jet, and potentially a more indirect effect of displacing the main-injection soot to regions where soot oxidation is enhanced.

The interaction between the post jet and the main-injection soot does not take place through only small-scale mixing, but also large-scale interaction of the post jet with the main-injection soot structures as the post jet initially penetrates into and past the main-injection soot. This interaction could be due to either large-scale displacement of the main-injection soot by the post jet, or rapid, progressive oxidation of the main-injection soot as a result of the penetration of the post jet. Additionally, images taken later in the cycle, near 375 CAD, have shown substantial differences in the spatial soot distribution between the single-injection and main- plus post-injection cases. Both of these pieces of evidence indicate that interaction of the post injection with main-injection soot is driving the soot reduction.

CONCLUSIONS

In this study, measurements of the spatial and temporal evolution of soot using high-speed imaging of soot natural luminosity (soot-NL) and planar-laser induced incandescence of soot (soot-PLII) in an optically accessible heavy-duty engine provide insight into the in-cylinder processes responsible for engine-out soot reduction with close-coupled post injections. Specific conclusions of this study are as follows:

1. Engine-out soot measurements unequivocally indicate that there is an interaction between the post jet and the main-injection soot, leading to a 20% reduction of engine-out soot compared to main-injection-only operation (and a 40% reduction at the same load). Although the magnitude of the soot reduction may change at other operating conditions [32], the low-load, moderate-EGR condition examined here is representative of current approaches to meet 2010 US on-road heavy-duty diesel-engine particulate and NO_x regulations [52] with the use of both urea-based selective catalytic reduction (SCR) and diesel particulate filter (DPF) after-treatment systems [3].
2. In-cylinder imaging shows evidence of early interaction of the post-injection with soot structures created by the main injection. Soot-PLII images show that as the post jet penetrates into the main-injection soot structures, the post-injection soot is initially quite distinct from the main-injection soot. The post- and main-injection soot structures are separated by a region of low soot concentration surrounding the post jet, especially in the upper half of the piston bowl. The separation is clearly evident in ensemble-averaged soot-PLII images, indicating that it occurs in most, if not all cycles. The "carving out" of the main-injection soot by the post injection could be due to either displacement or rapid oxidation; but the soot-PLII data are not sufficient to differentiate between these two mechanisms.
3. A few crank angle degrees after the initial interaction between the post jet and the main-injection soot structures, the high-speed soot-NL cinematographs also suggest merging of the post and main-injection soot, though line-of-sight uncertainties preclude definitive evidence of merging. Soot-PLII data, however, confirm that soot structures from the two injections become less distinct, merging together into a connected soot distribution within the soot-PLII laser sheets. Some of the merging may be due to entrainment of the main-injection products by the post injection [37].
4. A few more crank angle degrees later, the merged main- and post-injection soot spreads along the bowl wall. At the same time, main-injection soot outside the post-jet envelope decreases in concentration, especially in the lower soot-PLII sheets. By the time the fluid from the post jet reaches the lowest soot-PLII elevation (19 mm from the firedeck), most of the main-injection soot outside the post jet is already gone, whereas the soot remains nearly unchanged without the post injection. The in-plane soot reduction could be caused in part by the post injection displacing main-injection soot out of the laser sheet, but decreasing intensity in the line-of-sight integrated soot-NL images, as well as reduction of engine-out soot, strongly suggest that increased oxidation of the main-injection soot plays an important role.
5. Comparisons of soot-NL images with soot-PLII images acquired from multiple planar elevations along the line of sight for the soot-NL images show instances where intensity variations in soot luminosity must be interpreted with care. In some cases, strong intensity variations in soot-NL images do not agree with soot-PLII images, which show little variation. In other cases, significant differences in soot-PLII intensity are not apparent in soot-NL images.

Furthermore, late-cycle soot luminosity trends are not necessarily consistent with exhaust soot trends, in this case either with or without a post injection. These observations are consistent with a potential temperature bias to hotter combustion-heated soot in the soot-NL images, for which soot-PLII is less affected.

CLOSING COMMENTS ON FUTURE RESEARCH

Additional research to further elucidate the in-cylinder mechanisms of soot reduction would be helpful in two areas, described in the following two paragraphs: measurement of the

velocity field to understand more about the behavior of the post jet and its effect on the main-injection mixture, and characterization of soot oxidation processes.

In-cylinder velocity measurements would allow more precise tracking of the motion of the post jet as it penetrates into/past the slower-moving main-injection soot structures. The displacement of the main-injection mixture by the post jet, possible entrainment of the main-injection products into the post jet, and turbulent mixing at the interface between the post jet and main-injection soot would be more conclusively examined with velocity data.

Measurements of the high-temperature combustion and oxidation zones, for instance by planar-laser-induced fluorescence of OH (OH-PLIF) at multiple sheet elevations, would also be helpful. Such data would reveal the spatial extent of oxidation in the regions where soot concentrations rapidly decrease with post injections. Such evidence of soot oxidizing species would complement the velocity data to provide a more complete picture of how bulk displacement by the post injection and increased mixing in the vicinity of the post jet affect engine-out soot reduction. Such improved understanding could lead to better design of post-injection schedules and in-cylinder geometry for improved soot reduction performance with post injections.

REFERENCES

1. United States Environmental Protection Agency, “Fact sheet: Diesel exhaust in the United States” EPA420-F-03-022 (2003)
2. European Parliament, “Regulation (EC) No 595/2009 of 18 June 2009” (2009)
3. Cooper, B., Penny, I., Beasley, M., Greaney, A. et al., “Advanced Diesel Technology to Achieve Tier 2 Bin 5 Emissions Compliance in US Light-Duty Diesel Applications,” SAE Technical Paper 2006-01-1145, 2006, doi:10.4271/2006-01-1145.
4. Musculus M P B, Miles P C, Pickett L M, “Conceptual models for partially premixed low-temperature diesel combustion” Prog. Energy Combust. Sci. 39(2-3):246-283 (2013)
5. Dronniou, N., Lejeune, M., Balloul, I., and Higelin, P., “Combination of High EGR Rates and Multiple Injection Strategies to Reduce Pollutant Emissions,” SAE Technical Paper 2005-01-3726, 2005, doi:10.4271/2005-01-3726.
6. Montgomery, D. and Reitz, R., “Effects of Multiple Injections and Flexible Control of Boost and EGR on Emissions and Fuel Consumption of a Heavy-Duty Diesel Engine,” SAE Technical Paper 2001-01-0195, 2001, doi:10.4271/2001-01-0195.
7. O'Connor, J. and Musculus, M., “Post Injections for Soot Reduction in Diesel Engines: A Review of Current Understanding,” *SAE Int. J. Engines* 6(1):400-421, 2013, doi:10.4271/2013-01-0917.
8. Bobba, M., Musculus, M., and Neel, W., “Effect of Post Injections on In-Cylinder and Exhaust Soot for Low-Temperature Combustion in a Heavy-Duty Diesel Engine,” *SAE Int. J. Engines* 3(1):496-516, 2010, doi:10.4271/2010-01-0612.
9. Vanegas, A., Won, H., Felsch, C., Gauding, M. et al., “Experimental Investigation of the Effect of Multiple Injections on Pollutant Formation in a Common-Rail DI Diesel Engine,” SAE Technical Paper 2008-01-1191, 2008, doi:10.4271/2008-01-1191.
10. Mendez, S. and Thirouard, B., “Using Multiple Injection Strategies in Diesel Combustion: Potential to Improve Emissions, Noise and Fuel Economy Trade-Off in Low CR Engines,” *SAE Int. J. Fuels Lubr.* 1(1):662-674, 2009, doi:10.4271/2008-01-1329.
11. Zhang, Y. and Nishida, K., “Vapor/Liquid Behaviors in Split-Injection D.I. Diesel Sprays in a 2-D Model Combustion Chamber,” SAE Technical Paper 2003-01-1837, 2003, doi:10.4271/2003-01-1837.
12. Hotta, Y., Inayoshi, M., Nakakita, K., Fujiwara, K. et al., “Achieving Lower Exhaust Emissions and Better Performance in an HSDI Diesel Engine with Multiple Injection,” SAE Technical Paper 2005-01-0928, 2005, doi:10.4271/2005-01-0928.
13. Chen, S., “Simultaneous Reduction of NOx and Particulate Emissions by Using Multiple Injections in a Small Diesel Engine,” SAE Technical Paper 2000-01-3084, 2000, doi:10.4271/2000-01-3084.
14. Yun H, Sun Y, Reitz R D, “An experimental and numerical investigation on the effect of post injection strategies on combustion and emissions in the low- temperature diesel combustion regime” ICES2005-1043, ASME Internal Combustion Engine Division 2005 Spring Technical Conference, Chicago IL (2005)
15. Yun H and Reitz R D, “An experimental investigation on the effect of post-injection strategies on combustion and emissions in the low-temperature diesel combustion regime” J. Eng. Gas Turb. Power 129:279-286 (2007)
16. Tow, T., Pierpont, D., and Reitz, R., “Reducing Particulate and NOx Emissions by Using Multiple Injections in a Heavy Duty D.I. Diesel Engine,” SAE Technical Paper 940897, 1994, doi:10.4271/940897.
17. Pierpont, D., Montgomery, D., and Reitz, R., “Reducing Particulate and NOx Using Multiple Injections and EGR in a Diesel D.I.,” SAE Technical Paper 950217, 1995, doi:10.4271/950217.
18. Ehleskog, R. and Ochoterena, R., “Soot Evolution in Multiple Injection Diesel Flames,” SAE Technical Paper 2008-01-2470, 2008, doi:10.4271/2008-01-2470.
19. Barro C, Tschanz F, Obrecht P, Boulouchos K, “Influence of post-injection parameters on soot formation and oxidation in a common-rail-diesel engine using multi-color-pyrometry” ICEF2012-92075, ASME Internal Combustion Engine Division Fall Technical Conference, Vancouver BC (2012)
20. Sperl, A., “The Influence of Post-Injection Strategies on the Emissions of Soot and Particulate Matter in Heavy Duty Euro V Diesel Engine,” SAE Technical Paper 2011-36-0350, 2011, doi:10.4271/2011-36-0350.
21. Bakenhus, M. and Reitz, R., “Two-Color Combustion Visualization of Single and Split Injections in a Single-Cylinder Heavy-Duty D.I. Diesel Engine Using an Endoscope-Based Imaging System,” SAE Technical Paper 1999-01-1112, 1999, doi:10.4271/1999-01-1112.
22. Badami M, Mallamo F, Millo F, Rossi E, “Experimental investigation on the effect of multiple injection strategies on emissions, noise and brake specific fuel consumption of an automotive direct injection common-rail diesel engine” Int. J. Eng. Res. 4(4):299-314 (2003)
23. Benajes, J., Molina, S., and García, J., “Influence of Pre- and Post-Injection on the Performance and Pollutant Emissions in a HD Diesel Engine,” SAE Technical Paper 2001-01-0526, 2001, doi:10.4271/2001-01-0526.
24. Payri, F., Benajes, J., Pastor, J., and Molina, S., “Influence of the Post-Injection Pattern on Performance, Soot and NOx Emissions in a HD Diesel Engine,” SAE Technical Paper 2002-01-0502, 2002, doi:10.4271/2002-01-0502.
25. Helmantel A, Somhorst J, Denbratt I, “Visualization of the effects of post injection and swirl on the combustion process of a passenger car common rail DI diesel engine” ICES2003-622, Spring Technical Conference of ASME ICE Division, Salzberg Austria (2003)
26. Mancaruso E, Merola S, Vaglieco B, “Study of the multi-injection combustion process in a transparent direct injection common rail diesel engine by means of optical techniques” Int. J. Eng. Res. 9(6):483-498 (2008)
27. Bobba, M., Musculus, M., and Neel, W., “Effect of Post Injections on In-Cylinder and Exhaust Soot for Low-Temperature Combustion in a Heavy-Duty Diesel Engine,” *SAE Int. J. Engines* 3(1):496-516, 2010, doi:10.4271/2010-01-0612.
28. Han, Z., Uludogan, A., Hampson, G., and Reitz, R., “Mechanism of Soot and NOx Emission Reduction Using Multiple-injection in a Diesel Engine,” SAE Technical Paper 960633, 1996, doi:10.4271/960633.
29. Molina, S., Desantes, J., Garcia, A., and Pastor, J., “A Numerical Investigation on Combustion Characteristics with the use of Post Injection in DI Diesel Engines,” SAE Technical Paper 2010-01-1260, 2010, doi:10.4271/2010-01-1260.
30. Desantes, J., Arrègle, J., López, J., and García, A., “A Comprehensive Study of Diesel Combustion and Emissions with Post-injection,” SAE Technical Paper 2007-01-0915, 2007, doi:10.4271/2007-01-0915.

31. Beatrice C, Belardini P, Bertoli C, Lisbona M, Rossi Sebastiano G, "Diesel combustion control in common rail engines by new injection strategies" Int. J. Eng. Res. 3(1):23-36 (2002)
32. O'Connor J and Musculus M, "Effects of EGR and load on soot in a heavy-duty optical diesel engine with close-coupled post-injections for high efficiency combustion phasing" Int. J. Eng. Res. **in press** (2013)
33. Bruneaux G, "Liquid and vapor spray structure in high-pressure common rail diesel injection" Atomization and Sprays 11(5):533-556 (2001)
34. Bruneaux, G. and Maligne, D., "Study of the Mixing and Combustion Processes of Consecutive Short Double Diesel Injections," *SAE Int. J. Engines* 2(1):1151-1169, 2009, doi:10.4271/2009-01-1352.
35. Parrish, S., Zhang, G., and Zink, R., "Liquid and Vapor Envelopes of Sprays from a Multi-Hole Fuel Injector Operating under Closely-Spaced Double- Injection Conditions," *SAE Int. J. Engines* 5(2):400-414, 2012, doi:10.4271/2012-01-0462.
36. Genzale C L, *Optimizing combustion chamber design for low-temperature diesel combustion*, Department of Mechanical Engineering, University of Wisconsin - Madison (2008)
37. O'Connor, J and Musculus M P B, "Effect of load on close-coupled post-injection efficacy for soot reduction in an optical, heavy-duty diesel research engine" ICEF2013-19037 ASME Internal Combustion Engine Fall Technical Conference, Dearborn, MI (2013)
38. Hessel, R., Reitz, R., Musculus, M., O'Connor, J. et al., "A CFD Study of Post Injection Influences on Soot Formation and Oxidation under Diesel-like Operating Conditions," SAE Technical Paper 2014-01-1256, 2014, doi:10.4271/2014-01-1256.
39. Espey, C. and Dec, J., "Diesel Engine Combustion Studies in a Newly Designed Optical-Access Engine Using High-Speed Visualization and 2-D Laser Imaging," SAE Technical Paper 930971, 1993, doi:10.4271/930971.
40. Dec, J., "A Conceptual Model of DI Diesel Combustion Based on Laser-Sheet Imaging*," SAE Technical Paper 970873, 1997, doi:10.4271/970873.
41. Murphy M J, Taylor J D, McCormick R L, "Compendium of experimental cetane number data" National Renewable Energy Laboratory NREL/SR- 540-36805 (2004)
42. Bacha J, Freel J, Gibbs A, Heminghaus G, Hoekman K, Horn J, Ingham M, Jossens L, Kohler D, Lesnini D, McGeehan J, Nikanjam M, Olsen E, Scott B, Sztenderowicz M, Tiedemann A, Walker C, Lind J, Jones J, Scott D, Mills J, "Diesel Fuels Technical Review" Chevron Document MS-9915 (06-07) (2007)
43. Idicheria, C and Pickett L, "Ignition, soot formation, and end-of-combustion transients in diesel combustion under high-EGR conditions" Int. J. Engine Res. 12(4):376-392 (2011)
44. Heywood J B, *Internal combustion engine fundamentals*, McGraw-Hill, New York, NY (1988)
45. Musculus, M., "Effects of the In-Cylinder Environment on Diffusion Flame Lift-Off in a DI Diesel Engine," SAE Technical Paper 2003-01-0074, 2003, doi:10.4271/2003-01-0074.
46. Musculus, M., "On the Correlation between NOx Emissions and the Diesel Premixed Burn," SAE Technical Paper 2004-01-1401, 2004, doi:10.4271/2004-01-1401.
47. Kolodziej, C., Wirojsakunchai, E., Foster, D., Schmidt, N. et al., "Comprehensive Characterization of Particulate Emissions from Advanced Diesel Combustion," SAE Technical Paper 2007-01-1945, 2007, doi:10.4271/2007-01-1945.
48. Lilik, G K and Boehman A L, "Advanced diesel combustion of a high cetane number fuel with low hydrocarbon and carbon monoxide emissions" Energy & Fuels 25(4):1444-1456 (2011)
49. *Smoke value measurement with the filter-paper- method: Application notes*, AVL List GmbH: Graz, Austria (2005)
50. Cheng A, Upatnieks A, Mueller C J, "Investigation of fuel effects on dilute, mixing-controlled combustion in an optical direct-injection diesel engine" Energy & Fuels 21(4):1989-2002 (2007)
51. Mueller, C. and Martin, G., "Effects of Oxygenated Compounds on Combustion and Soot Evolution in a DI Diesel Engine:Broadband Natural Luminosity Imaging," SAE Technical Paper 2002-01-1631, 2002, doi:10.4271/2002-01-1631.
52. Chartier, C., Andersson, O., Johansson, B., Musculus, M. et al., "Effects of Post-Injection Strategies on Near-Injector Over-Lean Mixtures and Unburned Hydrocarbon Emission in a Heavy-Duty Optical Diesel Engine," *SAE Int. J. Engines* 4(1):1978-1992, 2011, doi:10.4271/2011-01-1383.
53. O'Connor, J and Musculus M P B, *Soot-NL video of instantaneous main-only and main- plus post- injection, 18% O_2, $SOI1_C$=347 CAD, $DOI1_C$=1550 microseconds, $SOI2_C$=366 CAD, $DOI2_C$=500 microseconds*. Available from: www.sandia.gov/ecn/pub-links/cdl/130208p130115l_instantaneous (2013)
54. O'Connor, J and Musculus M P B, *Soot-NL video of ensemble-average main-only and main- plus post- injection, 18% O_2, $SOI1_C$=347 CAD, $DOI1_C$=1550 microseconds, $SOI2_C$=366 CAD, $DOI2_C$=500 microseconds*=. Available from: www.sandia.gov/ecn/pub-links/cdl/130208p130115l_ensemble (2013)
55. Iglesias I, Vera M, Sánchez A L, Liñán A, "Simulations of starting gas jets at low Mach numbers" Physics of Fluids 17:038105 (2005)
56. Pickett, L M and Siebers D L, "Soot in diesel fuel jets: effects of ambient temperature, ambient density, and injection pressure" Combust. Flame 138(1):114-135 (2004)
57. Musculus, M. and Kattke, K., "Entrainment Waves in Diesel Jets," SAE Int. J. Engines 2(1):1170-1193, 2009, doi:10.4271/2009-01-1355.
58. *Engine Combustion Network Code*. Available from: http://www.sandia.gov/ecn/code.php (2013)

CONTACT INFORMATION

For more information, please contact:

Jacqueline O'Connor
Pennsylvania State University
jxo22@engr.psu.edu

ACKNOWLEDGEMENTS

The optical engine experiments were performed at the Combustion Research Facility, Sandia National Laboratories, Livermore, CA. Support for this research was provided by the U.S. Department of Energy, Office of Vehicle Technologies. Sandia is a multi-program laboratory operated by Sandia Corporation, a Lockheed Martin Company for the United States Department of Energy's National Nuclear Security Administration under contract DE-AC04-94AL85000. The authors gratefully acknowledge the contributions of Keith Penney and Dave Cicone for their assistance in maintaining the lasers and research engine used in this study. We also thank Randy Hessel at the University of Wisconsin for many fruitful discussions of post-injection behavior.

Definitions and Abbreviations

AHRR - Apparent heat release rate

C - Soot elemental carbon [mg/m3]

°CA - Duration measured in crank angle degrees

CAD - Crank angle degree position (360 CAD is TDC of compression stroke)

CMOS - Complementary metal oxide semiconductor

$DOI1_C$ - Commanded duration of main injection (in microseconds)

$DOI2_C$ - Commanded duration of post injection (in microseconds)

DPF - Diesel particulate filter

EGR - Exhaust gas recirculation

FSN - Filter smoke number

gIMEP - Gross indicated mean effective pressure

LTC - Low temperature combustion

OH-PLIF - OH planar laser induced fluorescence

PAH - Poly-cyclic aromatic hydrocarbon

RPM - Rotations per minute

SCR - Selective catalytic reduction

$SOI1_C$ - Commanded start of main injection (in crank angle degrees)

$SOI2_C$ - Commanded start of post injection (in crank angle degrees)

soot-NL - Soot natural luminosity

soot-PLII - Planar laser-induced incandescence of soot

TDC - Top dead center

UV - Ultra-violet

APPENDIX

Figure A1 provides a graphical reference that illustrates the estimated position of the post-jet relative to the piston bowl and laser sheets for the imaging sequences in Figs. 5, 6, 7, 8, 9. The post-injection penetration was estimated using the one-dimensional discrete control-volume jet model [57] from the Engine Combustion Network [58]. For the penetration calculations, the relevant model inputs were the dynamic injection velocity (changing with time) derived from the injection rate measurements (Fig. 3) assuming an orifice contraction coefficient of 0.83, an ambient density equal to the TDC motored density (16.6 kg/m3), and a full spreading angle of 17°. The illustrations in Fig. A1 show the nominal post-injection jet envelope using the same spreading angle. The widening usually observed at the head of penetrating jets is not illustrated in the figure, so the illustration may not depict the intersection of the actual jet envelope with the laser sheets. Similarly, expansion of the jet from heat release is not shown.

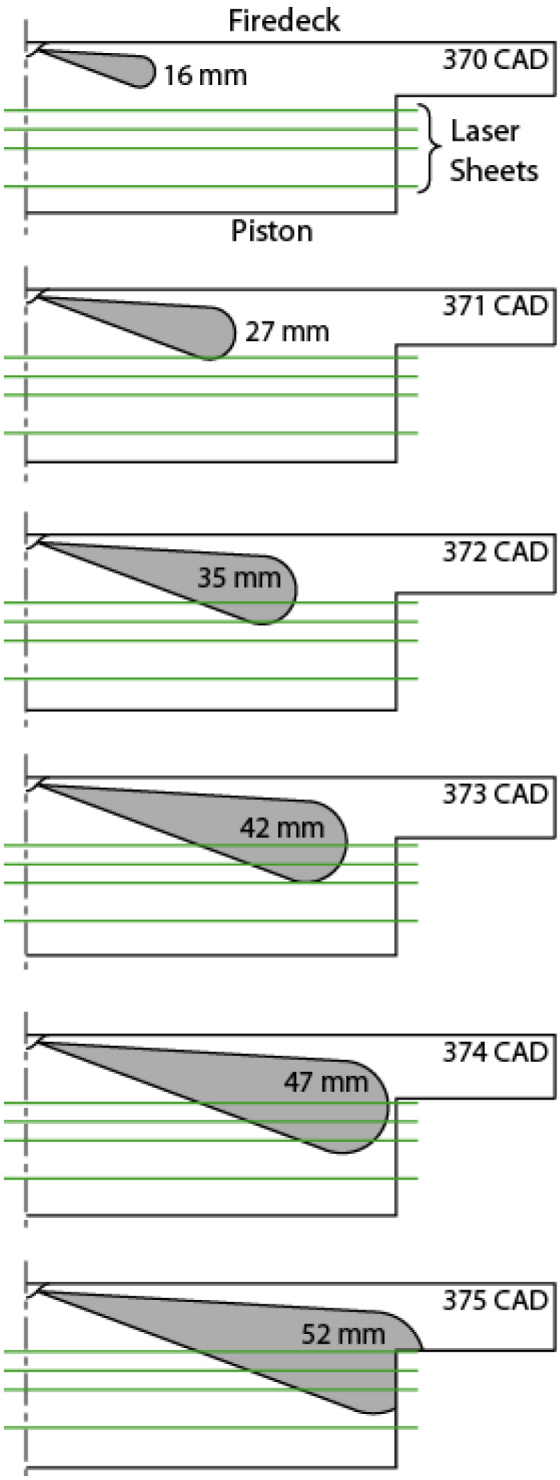

Figure A1. Estimated post-injection penetration and nominal jet envelope relative to soot-PLII laser sheets and piston geometry.